Optical undular bores in Riemann problem of photon fluid with quintic nonlinearity

Huan Gao and Deng-Shan Wang
Laboratory of Mathematics and Complex Systems (Ministry of Education), School of Mathematical Sciences, Beijing Normal University, Beijing 100875, China

(Received 12 April 2023; accepted 25 July 2023; published 25 August 2023)

This work develops the Whitham theory to study the Riemann problem of the Gerdjikov-Ivanov equation that describes the photon fluid with quintic nonlinearity. The one-phase periodic solution of the Gerdjikov-Ivanov equation and the corresponding Whitham equation are derived by the finite gap integration method. Subsequently, the main basic wave structures arising from the discontinuous initial-value conditions are found by distinguishing the distributions of the Riemann invariants. Some exotic optical undular bores are observed by classifying the solutions of the Riemann problem of the Gerdjikov-Ivanov equation. It is observed that the analytical results from Whitham theory are in excellent agreement with the numerical solutions.

DOI: 10.1103/PhysRevE.108.024222

I. INTRODUCTION

Undular bore (UB) describes the atmospheric wave phenomenon that occurs when a stable layer of air is disturbed. It is also called dispersive shock wave (DSW) in a dispersive hydrodynamic medium, which is the formation of fast oscillating nonlinear wave trains that spontaneously emerge from points of gradient catastrophe. The UBs or DSWs show up in certain physical systems such as shallow water wave motions [1], atmospheric science [2], tsunamis [3], ultracold atom systems [4], wave motions in magnetics [5], nonlinear optics [6,7], and plasma physics [8,9]. In particular, Fatome *et al.* [10] have observed the wave-breaking phenomenon and optical UBs in the multiple four-wave mixing of photon-fluid analogy.

Theoretically, the mathematical description of UB involves a combination of methods from hyperbolic quasilinear systems, which is represented as nonlinear periodic wave modulation. The formation and evolution process of UB is described by the Whitham theory [11,12], which was firstly proposed by Whitham in 1965 [11]. The derivation of the Whitham equation is the most important part of the Whitham theory for nonlinear wave equations, and currently there exist some effective methods, i.e., the Whitham's nonlinear averaging principle [13], perturbation expansion method [14,15], finite gap integration method [16], the averaged Lagrangian procedure [17], and so on. In the seminal work, Gurevich and Pitaevskii [13] explored the so-called Riemann problem of the Korteweg–de Vries equation and opened a way to study the discontinuous initial value problems of nonlinear wave equations by the Whitham theory.

The nonlinear Schrödinger (NLS) equation is one of the common soliton equations describing various physical problems such as nonlinear optics [18], surface gravity waves [19], superconductivity [20], and Bose-Einstein condensation [21]. In the direction of exploring DSW or UB of the NLS equation, important advances belonged to Gurevich [22–24] and his co-authors who applied the Whitham theory [11] to study the evolutions of the defocusing NLS equation under conditions of initial value discontinuity. In order to investigate the influence of NLS-type models under higher-order disturbances, researchers have made various modifications and generalizations to the NLS equation, among which three famous derivative nonlinear Schrödinger (DNLS) equations are proposed such as the Kaup-Newell equation [25], Chen-Lee-Liu equation [26], and Gerjikov-Ivanov equation [27], which are usually named as DNLS-I equation, DNLS-II equation, and DNLS-III equation, respectively. They appear in the theory of plasma physics, fluid dynamics, and nonlinear optics, etc.

In 1984, Kundu proposed [28] a generalized dimensionless quintic NLS equation

$$iq_t + q_{xx} + i\gamma(|q|^2 q)_x + i(\epsilon - 2\gamma)(|q|^2)_x q + \sigma|q|^4 q = 0, \tag{1}$$

where $q = q(x,t)$ is the complex envelope of an optical pulse, $\sigma = (\epsilon - \gamma)(\epsilon - 2\gamma)/4$ is the parameter of quintic nonlinearity often appeared in highly nonlinear materials such as organic polymers [29] and chalcogenide glasses [30], γ denotes for the pulse self-steepening effect, and ϵ relates to the nonlinearity dispersion. In the background of nonlinear optics, this equation can describe the transmission of ultrashort pulses in quadratic nonlinear medium considering the group-velocity mismatch [31]. Under special choice of the coefficients ϵ and γ, the generalized quintic NLS equation (1) can reduce to DNLS equations such as the Kaup-Newell equation for $\epsilon = 2\gamma$, the Chen-Lee-Liu equation for $\epsilon = \gamma$, and the following Gerjikov-Ivanov equation for $\epsilon = 0$, $\gamma = -1$:

$$iq_t + q_{xx} + iq^2 q_x^* + \tfrac{1}{2}|q|^4 q = 0. \tag{2}$$

In fact, there exist certain gauge transformations to relate the three DNLS equations and the solutions of each DNLS equation can be obtained from another one via the gauge transformations; however, it is difficult to get the explicit solution from the gauge transformations because of the indefinite integration involved in the transformations. Thus, it is necessary to study the three DNLS equations separately.

In recent years, various feasible approaches have been developed to study the Gerjikov-Ivanov equation (2). Fan [32] reexamined the complete integrability of this equation by proposing its Lax pair, bi-Hamiltonian structure and finite-dimensional integrable hierarchy. Biswas *et al.* [33] derived the conservation laws of the Gerdjikov-Ivanov equation by Lie symmetry analysis. Lü *et al.* [34] found the envelope bright- and dark-soliton solutions for the Gerdjikov-Ivanov equation based on the Madelung transformation. Fan [35] gave its solitonlike solutions by Darboux transformation. Xu *et al.* [36] considered the long-time asymptotic behaviors of the steplike initial-value problem. Moreover, Kudryashov [37] found some traveling-wave solutions of the Gerdjikov-Ivanov equation.

Ivanov and Kamchatnov [38] studied the Riemann problem of the Kaup-Newell equation that they named modified NLS equation and classified all the possible wave structures within the discontinuous jump conditions. Subsequently, Ivanov [39] himself investigated the Riemann problem of the general Chen-Lee-Liu equation modeling the fiber optical pulse by Whitham theory. Therefore, this work focuses on the evolutions of initial discontinuity of the Gerdjikov-Ivanov equation (2) by investigating the modulated periodic solutions and the complete classification of all possible solutions of the steplike initial data.

The structure of this paper is organized as follows: the one-phase periodic solution and the corresponding Whitham equation are derived by the finite gap integration method in Section 2. In Section 3, the elementary wave structures under the condition of initial discontinuity are found, i.e., the rarefaction waves, the cnoidal dispersive shock waves, the contact dispersive shock waves, and the combined waves. Section 4 classifies the solutions of the Riemann problem and compares the numerical solutions with the findings of the Whitham theory. The conclusions are proposed in the last section.

II. ONE-PHASE PERIODIC SOLUTION AND WHITHAM EQUATIONS

The Gerdjikov-Ivanov equation (2) is the compatibility condition of the following linear spectral problem [32]:

$$\Psi_x = \begin{pmatrix} F & G \\ H & -F \end{pmatrix}\Psi, \tag{3}$$

$$\Psi_t = \begin{pmatrix} A & B \\ C & -A \end{pmatrix}\Psi, \tag{4}$$

where $\Psi = (\psi_1(x,t), \psi_2(x,t))^T,\ q = q(x,t)$, and

$$\begin{aligned} F &= -ik^2 - \frac{i}{2}|q|^2, \quad G = kq, \quad H = kq^*, \\ A &= -2ik^4 - ik^2|q|^2 + \frac{i}{4}|q|^4 - \frac{1}{2}qq_x^* + \frac{1}{2}q^*q_x, \\ B &= 2k^3q + ikq_x, \quad C = 2k^3q^* - ikq_x^*, \end{aligned} \tag{5}$$

with the spectral parameter $k \in \mathbb{C}$.

Assume $(\psi_1(x,t), \psi_2(x,t))^T$ and $(\varphi_1(x,t), \varphi_2(x,t))^T$ are the two linearly independent basis solutions of the linear problems (3) and (4), then define the "squared basis functions" [7,40,41] as

$$f = -\frac{i}{2}(\psi_1\varphi_2 + \psi_2\varphi_1), \quad g = \psi_1\varphi_1, \quad h = -\psi_2\varphi_2. \tag{6}$$

It is convenient to check that f, g, h satisfy the linear equations

$$\begin{aligned} f_x &= iGh - iHg, \\ g_x &= 2iGf + 2Fg, \\ h_x &= -2iHf - 2Fh, \end{aligned} \tag{7}$$

and

$$\begin{aligned} f_t &= -iCg + iBh, \\ g_t &= 2iBf + 2Ag, \\ h_t &= -2iCf - 2Ah. \end{aligned} \tag{8}$$

It is remarked that by using the algebro-geometrical approach given in the Refs. [41,42] and the book [43], the N-phase algebro-geometric solutions of the Gerdjikov-Ivanov equation (2) can be obtained directly. However, to study the Riemann problem of the Gerdjikov-Ivanov equation (2), we only need the one-phase periodic solution. Thus following the procedure of the finite gap integration method [16], this section focuses on the one-phase periodic solution and the corresponding Whitham equations associated with the Gerdjikov-Ivanov equation (2). To do so, take

$$\begin{aligned} f &= \left(k^2 + \tfrac{1}{4}|q|^2\right)^2 - f_1\left(k^2 + \tfrac{1}{4}|q|^2\right) + f_2, \\ g &= (k^2 - \mu)qk, \\ h &= (k^2 - \mu^*)q^*k, \end{aligned} \tag{9}$$

where $f_1,\ f_2,\ \mu(x,t)$, and $\mu^*(x,t)$ are functions to be determined below, and the function $\mu^*(x,t)$ is the complex conjugate of the function $\mu(x,t)$.

Substituting (9) into (7) and comparing the coefficients on the powers of k yield

$$f_{1x} = 0, \quad f_{2x} = -\frac{1}{4}\left(\frac{|q|^2}{2} + f_1\right)(|q|^2)_x, \tag{10}$$

$$\begin{aligned} &(|q|^2)_x = 2i|q|^2(\mu - \mu^*), \quad q_x = -2iqf_1 + 2iq\mu, \\ &(\mu q)_x = -\frac{i}{8}|q|^4q + \frac{i}{2}|q|^2qf_1 - i|q|^2q\mu - 2if_2q. \end{aligned} \tag{11}$$

Similarly, substituting (9) into (8) yields

$$f_{1t} = 0, \quad f_{2t} = 2f_1f_{2x}, \quad (|q|^2)_t = 2f_1|q|_x^2. \tag{12}$$

It can be proved that the quantity $f^2 - gh = -\frac{1}{4}(\psi_1\varphi_2 - \psi_2\varphi_1)^2$ is independent of x and t and is a polynomial of parameter k. When considering the one-phase periodic solution, the $f^2 - gh$ can be expressed by

$$\begin{aligned} f^2 - gh = P(k) &= \prod_{j=1}^{4}\left(k^2 - k_j^2\right) \\ &= k^8 - s_1k^6 + s_2k^4 - s_3k^2 + s_4. \end{aligned} \tag{13}$$

Comparing the coefficients of the powers in k on both sides of Eq. (13), one obtains

$$s_1 = 2f_1, \tag{14}$$

$$s_2 = f_1^2 + 2f_2 + \tfrac{3}{8}|q|^4 - \tfrac{3}{2}f_1|q|^2 + |q|^2(\mu + \mu^*), \tag{15}$$

$$s_3 = 2f_1f_2 - \tfrac{1}{16}|q|^6 + \tfrac{3}{8}|q|^4 f_1 + |q|^2\left(\mu\mu^* - f_2 - \tfrac{1}{2}f_1^2\right), \tag{16}$$

$$s_4 = \left[\left(\tfrac{1}{4}|q|^2 - f_1\right)\tfrac{1}{4}|q|^2 + f_2\right]^2. \tag{17}$$

On the other side, we have

$$s_1 = \sum_{j=1}^{4} k_j^2, \quad s_2 = \sum_{i<j} k_i^2 k_j^2,$$
$$s_3 = \sum_{i<j<s} k_i^2 k_j^2 k_s^2, \quad s_4 = k_1^2k_2^2k_3^2k_4^2. \tag{18}$$

Obviously, Eqs. (14) and (17) imply

$$f_1 = \frac{s_1}{2}, \quad f_2 = \pm\sqrt{s_4} - \frac{|q|^4}{16} + \frac{s_1}{8}|q|^2. \tag{19}$$

Combining Eqs. (16) and (17) and noticing $\rho = |q|^2$, the expression of the function μ is determined as

$$\mu = \frac{1}{8\rho}[2s_1\rho - \rho^2 + 4s_2 - s_1^2 \mp 8\sqrt{s_4} - i\sqrt{-R(\rho)}], \tag{20}$$

where

$$\begin{aligned} R(\rho) = {} & \rho^4 - 4s_1\rho^3 - \left(8s_2 - 6s_1^2 \pm 48\sqrt{s_4}\right)\rho^2 \\ & + \left(16s_1s_2 - 4s_1^3 - 64s_3 \pm 32\sqrt{s_4}\right)\rho \\ & + \left(s_1^2 - 4s_2 \pm 8\sqrt{s_4}\right)^2. \end{aligned} \tag{21}$$

The signs "$\pm$" associate with sheets of the Riemann surface $R(\rho)$. In addition, $R(\rho)$ describes an algebraic resolvent of $P(k)$. According to the fundamental theorem of algebra, $R(\rho)$ has four complex roots, which can be expressed by roots of $P(k)$. In this way, the roots related to the lower sign (–) can be represented as

$$\begin{aligned} \rho_1 &= (k_2 - k_1 + k_3 + k_4)^2, \\ \rho_2 &= (k_1 - k_2 + k_3 + k_4)^2, \\ \rho_3 &= (k_1 + k_2 - k_3 + k_4)^2, \\ \rho_4 &= (k_1 + k_2 + k_3 - k_4)^2. \end{aligned} \tag{22}$$

In this similar way, the roots related to the upper sign (+) can be represented as

$$\begin{aligned} \rho_1 &= (k_2 - k_1 + k_3 - k_4)^2, \\ \rho_2 &= (k_1 - k_2 + k_3 - k_4)^2, \\ \rho_3 &= (k_1 + k_2 - k_3 - k_4)^2, \\ \rho_4 &= (k_1 + k_2 + k_3 + k_4)^2. \end{aligned} \tag{23}$$

The traveling-wave transformation

$$\xi = x - Vt, \quad V = -2f_1 = -s_1 = -\tfrac{1}{4}\Sigma_{j=1}^4 \rho_j \tag{24}$$

and $f_2(x,t) = f_2(\xi)$, $\rho(x,t) = \rho(\xi)$ indicate that

$$\frac{d\rho(\xi)}{d\xi} = \frac{1}{2}\sqrt{-R(\rho)}. \tag{25}$$

For simplicity, set $k_1 \leqslant k_2 \leqslant k_3 \leqslant k_4 \leqslant 0$, which means that $\rho_1 \leqslant \rho_2 \leqslant \rho_3 \leqslant \rho_4$. It is reasonable to consider the two intervals

$$\rho_1 \leqslant \rho \leqslant \rho_2, \quad \rho_3 \leqslant \rho \leqslant \rho_4, \tag{26}$$

which may produce two one-phase periodic solutions in terms of Jacobi elliptic functions for Eq. (25).

Firstly, for $\rho_1 \leqslant \rho \leqslant \rho_2$, the one-phase periodic solution is

$$\rho = \frac{\rho_2(\rho_4 - \rho_1) - \rho_4(\rho_2 - \rho_1)\mathrm{cn}^2(\omega, m)}{\rho_4 - \rho_2 + (\rho_2 - \rho_1)\mathrm{sn}^2(\omega, m)}, \tag{27}$$

with the wavelength

$$L = \frac{8K(m)}{\sqrt{(\rho_3 - \rho_1)(\rho_4 - v_2)}} = \frac{2K(m)}{\sqrt{(k_3^2 - k_1^2)(k_4^2 - k_2^2)}}, \tag{28}$$

and the parameters

$$\omega = \tfrac{1}{4}\sqrt{(\rho_3 - \rho_1)(\rho_4 - \rho_2)}\xi, \tag{29}$$

$$m = \frac{(\rho_4 - \rho_3)(\rho_2 - \rho_1)}{(\rho_4 - \rho_2)(\rho_3 - \rho_1)} = \frac{\left(k_4^2 - k_3^2\right)\left(k_2^2 - k_1^2\right)}{\left(k_4^2 - k_2^2\right)\left(k_3^2 - k_1^2\right)}, \tag{30}$$

where the functions cn and sn are Jacobi elliptic functions, and $K(m)$ is the complete elliptic integral of the first kind [44].

One should analyze the special cases of the one-phase periodic solution (27) in different limits. In doing so, the limit of $m \to 1$ (i.e., $\rho_3 \to \rho_2$) results in the bright soliton

$$\rho = \frac{\rho_1(\rho_4 - \rho_2) + \rho_4(\rho_2 - \rho_1)\tanh^2(\omega_1)}{\rho_4 - \rho_2 + (\rho_2 - \rho_1)\tanh^2(\omega_1)}, \tag{31}$$

where $\omega_1 = \sqrt{(\rho_2 - \rho_1)(\rho_4 - \rho_2)}\xi/4$.

In the limit $m \to 0$, there are two ways to analyze the degeneration of the one-phase periodic solution (27), which are $\rho_2 \to \rho_1$ and $\rho_4 \to \rho_3$, respectively. For the case $\rho_2 \to \rho_1$, the one-phase periodic solution (27) degenerates into a constant solution

$$\rho = \rho_2, \tag{32}$$

while for the case $\rho_4 \to \rho_3$, the one-phase periodic solution (27) degenerates into a trigonometric wave solution

$$\rho = \frac{\rho_2(\rho_3 - \rho_1) - \rho_3(\rho_2 - \rho_1)\cos^2(\omega_0)}{\rho_3 - \rho_2 + (\rho_2 - \rho_1)\sin^2(\omega_0)}, \tag{33}$$

with $\omega_0 = \sqrt{(\rho_3 - \rho_1)(\rho_3 - \rho_2)}\xi/4$.

Similarly, for $\rho_3 \leqslant \rho \leqslant \rho_4$, another one-phase periodic solution of (25) is

$$\rho = \frac{\rho_3(\rho_1 - \rho_4) + \rho_1(\rho_4 - \rho_3)\mathrm{cn}^2(\omega, m)}{\rho_1 - \rho_3 + (\rho_3 - \rho_4)\mathrm{sn}^2(\omega, m)}, \tag{34}$$

where L, ω, m are given in (28)–(30).

In the soliton limit $m \to 1$ (i.e., $\rho_2 \to \rho_3$), the one-phase periodic solution (34) degenerates into the dark-soliton solution

$$\rho = \frac{\rho_3(\rho_1 - \rho_4) - \rho_1(\rho_3 - \rho_4)\mathrm{sech}^2(\omega)}{\rho_1 - \rho_4 + (\rho_4 - \rho_3)\mathrm{sech}^2(\omega)}. \tag{35}$$

By analogy, the limit $m \to 0$ indicates that $\rho_2 \to \rho_1$ or $\rho_4 \to \rho_3$. In the case of $\rho_4 \to \rho_3$, the one-phase periodic solution (34) degenerates into a constant solution

$$\rho = \rho_3, \tag{36}$$

while for the case $\rho_2 \to \rho_1$, the one-phase periodic solution (34) degenerates into a trigonometric wave solution

$$\rho = \frac{\rho_3(\rho_1 - \rho_4) + \rho_1(\rho_4 - \rho_3)\cos^2(\omega)}{\rho_1 - \rho_3 + (\rho_3 - \rho_4)\sin^2(\omega)}. \tag{37}$$

Moreover, constraining the limit $\rho_3 \to \rho_2 = \rho_1$ leads to the algebraic soliton solution of the form

$$\rho = \rho_1 + \frac{16(\rho_4 - \rho_1)}{16 + (\rho_4 - \rho_1)^2\xi^2}. \tag{38}$$

In what follows, the Whitham theory [7] is adopted to modulate the one-phase periodic solutions in (27) and (34). To do so, it is necessary to derive the conservation laws of the Gerjikov-Ivanov equation (2), normalize the squared eigenfunctions f, g, and h and then average the generating function of the conservation laws to derive the Whitham equations. Substituting the equations in (7) and (8) into

$$(\log g)_{xt} = (\log g)_{tx} \tag{39}$$

derives the conservation law

$$\left(\frac{G}{g}\right)_t = \left(\frac{B}{g}\right)_x. \tag{40}$$

The scale transformation

$$f \to \frac{f}{\sqrt{P(k)}}, \quad g \to \frac{g}{\sqrt{P(k)}}, \quad h \to \frac{h}{\sqrt{P(k)}} \tag{41}$$

normalizes the condition $f^2 - gh = P(k)$ as

$$\left(\frac{f}{\sqrt{P(k)}}\right)^2 - \frac{g}{\sqrt{P(k)}}\frac{h}{\sqrt{P(k)}} = 1. \tag{42}$$

The conservation law (40) can be modified as

$$\left(\sqrt{P(k)}\frac{G}{g}\right)_t = \left(\sqrt{P(k)}\frac{B}{g}\right)_x. \tag{43}$$

Averaging of Eq. (43) over the wavelength L and noticing the differential form

$$dx = \frac{d\mu}{2\sqrt{-P(\sqrt{\mu})}},$$

the averaged conservation law [7] is obtained as

$$\left(\frac{\sqrt{P(k)}}{2L}\oint \frac{d\mu}{2(k^2-\mu)\sqrt{-P(\sqrt{\mu})}}\right)_t \tag{44}$$

$$= \left[\frac{\sqrt{P(k)}}{2L}\oint\left(2 + \frac{2f_1}{k^2-\mu}\right)\frac{d\mu}{2\sqrt{-P(\sqrt{\mu})}}\right]_x. \tag{45}$$

Taking the limit $k \to k_i$ $(i = 1, 2, 3, 4)$ yields

$$\oint \frac{d\mu}{2(k_i^2-\mu)\sqrt{-P(\sqrt{\mu})}}\frac{\partial k_i}{\partial t} = \oint\left(2 + \frac{2f_1}{k_i^2-\mu}\right)\frac{d\mu}{2\sqrt{-P(\sqrt{\mu})}}\frac{\partial k_i}{\partial x},$$

which results in the Whitham equation for the Riemannn invariants k_i for $(i = 1, 2, 3, 4)$ below:

$$\frac{\partial k_i}{\partial t} + v_i\frac{\partial k_i}{\partial x} = 0, \quad i = 1, 2, 3, 4, \tag{46}$$

where the characteristic velocities v_i are given by

$$\begin{aligned} v_i &= -\frac{I_2(k_i)}{I_1(k_i)} = V + \frac{1}{\frac{\partial \ln(L)}{\partial k_i^2}}, \quad i = 1, 2, 3, 4,\\ I_1 &= \oint \frac{d\mu}{2(k_i^2-\mu)\sqrt{-P(\sqrt{\mu})}} = -2\frac{\partial L}{\partial k_i^2},\\ I_2 &= \oint\left(2 + \frac{2f_1}{k_i^2-\mu}\right)\frac{d\mu}{2\sqrt{-P(\sqrt{\mu})}} = 2L + s_1 I_1. \end{aligned} \tag{47}$$

After some calculations, the exact representations of the characteristic velocities v_i $(i = 1, 2, 3, 4)$ are expressed by

$$\begin{aligned} v_1 &= -\sum_{i=1}^{4} k_i^2 - \frac{2(k_1^2-k_2^2)(k_1^2-k_4^2)K(m)}{(k_1^2-k_4^2)K(m) - (k_2^2-k_4^2)E(m)},\\ v_2 &= -\sum_{i=1}^{4} k_i^2 - \frac{2(k_1^2-k_2^2)(k_2^2-k_3^2)K(m)}{(k_3^2-k_2^2)K(m) + (k_1^2-k_3^2)E(m)},\\ v_3 &= -\sum_{i=1}^{4} k_i^2 + \frac{2(k_3^2-k_4^2)(k_2^2-k_3^2)K(m)}{(k_3^2-k_2^2)K(m) + (k_2^2-k_4^2)E(m)},\\ v_4 &= -\sum_{i=1}^{4} k_i^2 - \frac{2(k_3^2-k_4^2)(k_1^2-k_4^2)K(m)}{(k_4^2-k_1^2)K(m) + (k_1^2-k_3^2)E(m)}, \end{aligned} \tag{48}$$

where $K(m)$ and $E(m)$ are the complete elliptic integrals of the first and second kind, respectively.

Next define the new Riemann invariants of the form

$$\lambda_i = -k_i^2. \tag{49}$$

The inequality $k_4 \leqslant k_3 \leqslant k_2 \leqslant k_1 \leqslant 0$ indicates that $\lambda_4 \leqslant \lambda_3 \leqslant \lambda_2 \leqslant \lambda_1 \leqslant 0$, which shows that the characteristic velocities v_i $(i = 1, 2, 3, 4)$ can be expressed in terms of λ_i as

$$\begin{aligned} v_1 &= (-\sqrt{-\lambda_1} + \sqrt{-\lambda_2} + \sqrt{-\lambda_3} - \sqrt{-\lambda_4})^2,\\ v_2 &= (\sqrt{-\lambda_1} - \sqrt{-\lambda_2} + \sqrt{-\lambda_3} - \sqrt{-\lambda_4})^2,\\ v_3 &= (\sqrt{-\lambda_1} + \sqrt{-\lambda_2} - \sqrt{-\lambda_3} - \sqrt{-\lambda_4})^2,\\ v_4 &= (\sqrt{-\lambda_1} + \sqrt{-\lambda_2} + \sqrt{-\lambda_3} + \sqrt{-\lambda_4})^2 \end{aligned} \tag{50}$$

or

$$\begin{aligned} v_1 &= (\sqrt{-\lambda_1} + \sqrt{-\lambda_2} + \sqrt{-\lambda_3} - \sqrt{-\lambda_4})^2,\\ v_2 &= (\sqrt{-\lambda_1} + \sqrt{-\lambda_2} - \sqrt{-\lambda_3} + \sqrt{-\lambda_4})^2,\\ v_3 &= (\sqrt{-\lambda_1} - \sqrt{-\lambda_2} + \sqrt{-\lambda_3} + \sqrt{-\lambda_4})^2,\\ v_4 &= (-\sqrt{-\lambda_1} + \sqrt{-\lambda_2} + \sqrt{-\lambda_3} + \sqrt{-\lambda_4})^2. \end{aligned} \tag{51}$$

In this case, the velocity V, the wavelength L, and the modulus m can be rewritten as

$$V = \Sigma_{j=1}^{4}\lambda_j, \quad L = \frac{8K(m)}{\sqrt{(\lambda_3-\lambda_1)(\lambda_4-\lambda_2)}}, \tag{52}$$

$$m = \frac{(\lambda_4-\lambda_3)(\lambda_2-\lambda_1)}{(\lambda_4-\lambda_2)(\lambda_3-\lambda_1)}. \tag{53}$$

In addition, the Whitham equation for the Riemannn invariants λ_i $(i = 1, 2, 3, 4)$ are expressed by

$$\frac{\partial\lambda_i}{\partial t} + \nu_i\frac{\partial\lambda_i}{\partial x} = 0, \quad \nu_i = V - \frac{1}{\frac{\partial \ln(L)}{\partial\lambda_i}}, \quad i = 1, 2, 3, 4, \tag{54}$$

with the characteristic velocities

$$\begin{aligned}
\nu_1 &= \sum_{i=1}^{4}\lambda_i + \frac{2(\lambda_1-\lambda_2)(\lambda_1-r_4)K(m)}{(\lambda_1-\lambda_4)K(m)-(\lambda_2-\lambda_4)E(m)},\\
\nu_2 &= \sum_{i=1}^{4}\lambda_i + \frac{2(\lambda_1-\lambda_2)(\lambda_2-\lambda_3)K(m)}{(\lambda_3-\lambda_2)K(m)+(\lambda_1-\lambda_3)E(m)},\\
\nu_3 &= \sum_{i=1}^{4}\lambda_i - \frac{2(\lambda_3-\lambda_4)(\lambda_2-\lambda_3)K(m)}{(\lambda_3-\lambda_2)K(m)+(\lambda_2-\lambda_4)E(m)},\\
\nu_4 &= \sum_{i=1}^{4}\lambda_i + \frac{2(\lambda_3-\lambda_4)(\lambda_1-\lambda_4)K(m)}{(\lambda_4-\lambda_1)K(m)+(\lambda_1-\lambda_3)E(m)}.
\end{aligned} \tag{55}$$

In the similar way as [7], one can also consider the limits of the characteristic velocities ν_i $(i = 1, 2, 3, 4)$. For the case $m \to 1$ (i.e., $\lambda_3 \to \lambda_2$), the Whitham velocities ν_i $(i = 1, 2, 3, 4)$ degenerate into

$$\begin{aligned}
\nu_1 &= 3\lambda_1 + \lambda_4,\\
\nu_2 &= \nu_3 = \lambda_1 + 2\lambda_2 + \lambda_4,\\
\nu_4 &= \lambda_1 + 3\lambda_4.
\end{aligned} \tag{56}$$

In the harmonic front $m \to 0$ (i.e., $\lambda_4 \to \lambda_3$), the Whitham velocities ν_i $(i = 1, 2, 3, 4)$ degenerate into

$$\begin{aligned}
\nu_1 &= 3\lambda_1 + \lambda_2,\\
\nu_2 &= \lambda_1 + 3\lambda_2,\\
\nu_3 &= \nu_4 = 4\lambda_3 + \frac{(\lambda_1-\lambda_2)^2}{\lambda_1+\lambda_2-2\lambda_3}.
\end{aligned} \tag{57}$$

Moreover, in another limit state $m \to 0$ (i.e., $\lambda_2 \to \lambda_1$), the Whitham velocities ν_i $(i = 1, 2, 3, 4)$ degenerate into

$$\begin{aligned}
\nu_1 &= \nu_2 = 4\lambda_1 + \frac{(\lambda_4-\lambda_3)^2}{2\lambda_1-\lambda_3-\lambda_4},\\
\nu_3 &= 3\lambda_3 + \lambda_4,\\
\nu_4 &= \lambda_3 + 3\lambda_4.
\end{aligned} \tag{58}$$

III. KEY ELEMENTS OF SELF-SIMILAR WAVE STRUCTURES

This work focuses on the Riemann problem of the Gerdjikov-Ivanov equation (2), which corresponds to the discontinuous initial value condition [45,46]

$$q(x,0) = \sqrt{\rho}e^{i\phi}, \quad \phi_x = w \tag{59}$$

with $\rho = \rho(x, 0)$ and $w = w(x, 0)$ satisfying

$$\rho(x,0) = \begin{cases}\rho_L, & x<0\\ \rho_R, & x>0,\end{cases} \quad w(x,0) = \begin{cases}w_L, & x<0\\ w_R, & x>0,\end{cases} \tag{60}$$

where ρ_L, ρ_R, w_L, and w_R are real constants. First of all, the basic wave structures of the Gerdjikov-Ivanov equation under the initial value condition (59) with (60) should be clarified.

A. The rarefaction waves

Taking the Madelung transformation [38,39]

$$q = \sqrt{\rho}e^{i\phi}, \quad \phi_x = w, \tag{61}$$

where $\rho = \rho(x, t)$ and $w = w(x, t)$ are the fluid density and fluid velocity, respectively, the hydrodynamic form of the Gerdjikov-Ivanov equation (2) is

$$\begin{aligned}
&\rho_t + 2\rho_x w + 2\rho w_x + \rho\rho_x = 0,\\
&w_t + 2ww_x - (\rho w)_x - \rho\rho_x = \frac{1}{\sqrt{\rho}}\left(\frac{\rho_{xx}}{2\sqrt{\rho}} - \frac{\rho_x^2}{4\rho^{\frac{3}{2}}}\right)_x.
\end{aligned} \tag{62}$$

The traveling-wave solution of the hydrodynamic-type equation (62) is studied in the Appendix, where the explicit exact solutions of fluid density ρ and fluid velocity w are proposed.

Dropping the high-order dispersion term in the second equation of the system (62), the dispersionless equation is obtained as

$$\begin{pmatrix} w\\ \rho\end{pmatrix}_t = \begin{pmatrix}\rho-2w & \rho+w\\ -2\rho & -\rho-2w\end{pmatrix}\begin{pmatrix} w\\ \rho\end{pmatrix}_x, \tag{63}$$

whose characteristic equation is

$$\xi^2 + 4w\xi + 4w^2 + 2\rho w + \rho^2 = 0, \tag{64}$$

where ξ is the eigenvalue. The discriminant of the quadratic equation (64) is $\Delta = -4\rho(2w + \rho)$. If $2w + \rho < 0$, there are two different real roots, which corresponds to a hyperbolic system. Since the conservation law for $w = \phi_x$ is trivial, it is necessary to look for another conserved density without the derivatives of x. Therefore, replacing ρ with the variable $\hat{\rho} = -\rho^2 - 2\rho w$ [47] such that

$$\rho = -w \pm \sqrt{w^2 - \hat{\rho}}, \tag{65}$$

then the dispersionless equation (63) becomes

$$\begin{pmatrix} \hat{\rho}\\ w\end{pmatrix}_t = \begin{pmatrix}-2w & -2\hat{\rho}\\ -\frac{1}{2} & -2w\end{pmatrix}\begin{pmatrix} \hat{\rho}\\ w\end{pmatrix}_x, \tag{66}$$

which can be written as diagonal form

$$\frac{\partial r_\pm}{\partial t} + \upsilon_\pm\frac{\partial r_\pm}{\partial x} = 0, \tag{67}$$

where the Riemann invariants $r_\pm$ and the characteristic velocities $\upsilon_\pm$ take the form

$$r_\pm = w \pm \sqrt{\hat{\rho}} = w \pm \sqrt{-\rho(\rho+2w)}, \tag{68}$$

$$\upsilon_\pm = 2w \pm \sqrt{\hat{\rho}} = 2w \pm \sqrt{-\rho(\rho+2w)}. \tag{69}$$

It is easy to see

$$\upsilon_+ = \tfrac{3}{2}r_+ + \tfrac{1}{2}r_-, \quad \upsilon_- = \tfrac{1}{2}r_+ + \tfrac{3}{2}r_-, \tag{70}$$

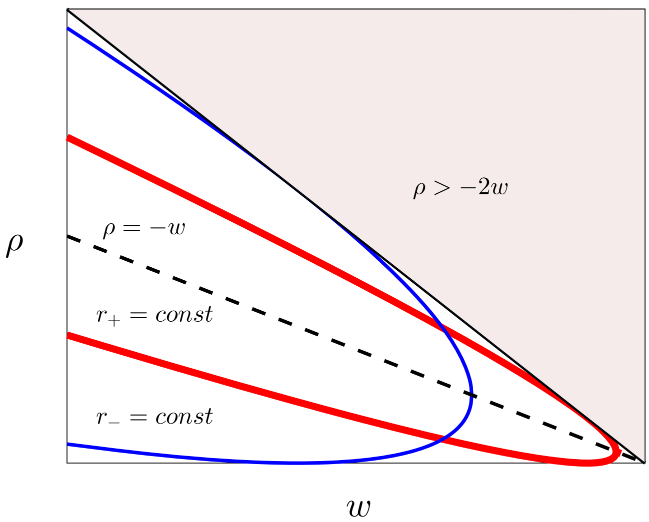

FIG. 1. The curves formed by the relationship between ρ and w, where the gray area corresponds to the modulational instability state for $\rho > -2w$ and the black dotted line represents $\rho = -w$.

and the trace formulas for the functions ρ and w are

$$\rho = -\tfrac{1}{2}(r_+ + r_-) \pm \sqrt{r_+ r_-}, \quad w = \tfrac{1}{2}(r_+ + r_-), \tag{71}$$

where the Riemann invariants $r_\pm$ are nonpositive, i.e., $r_- \leqslant r_+ \leqslant 0$.

In what follows, the rarefaction wave solutions are investigated in detail, which means one of the Riemann invariants is constant, i.e., $r_+ = \text{const}$ or $r_- = \text{const}$. Equation (68) denotes that the variable ρ can be expressed as w and $r_\pm$ of the form

$$\rho = -w \pm \sqrt{r_\pm(2w - r_\pm)}, \tag{72}$$

which is displayed in Fig. 1. Along the line $\rho = -w$, one notices that $\partial r_+/\partial w = 0$, $\partial r_+/\partial \rho = 0$. And this line separates two monotonic regions in the plane (w, ρ) (see Fig. 1). In Fig.1, the red (thick) curve corresponds to the case that r_+ is constant, while the blue (thin) curve corresponds to the case that r_- is constant. At the two intersection points of curves, $r_\pm = \text{const}$, this denotes that ρ and w are constants by Eq. (72), which corresponds to the trivial plateau solutions of the Gerdjikov-Ivanov equation (2).

Considering the self-similar variable $\xi = x/t$ as in [38,39], one obtains $r_\pm = r_\pm(\xi)$ and the Whitham equation (67) is converted into

$$(\upsilon_+ - \xi)\frac{dr_+}{d\xi} = 0, \quad (\upsilon_- - \xi)\frac{dr_-}{d\xi} = 0. \tag{73}$$

Obviously, the equations in (73) have trivial constant solutions, i.e., $r_\pm = \text{const}$, which corresponds to the plateau solution discussed above. What is more, two types of rarefaction wave solution are obtained below:

$$\begin{aligned} &(a) \quad r_- = \text{const} \equiv r_-^0, \quad \upsilon_+ = \tfrac{3}{2}r_+ + \tfrac{1}{2}r_- = \xi, \\ &(b) \quad r_+ = \text{const} \equiv r_+^0, \quad \upsilon_- = \tfrac{1}{2}r_+ + \tfrac{3}{2}r_- = \xi. \end{aligned} \tag{74}$$

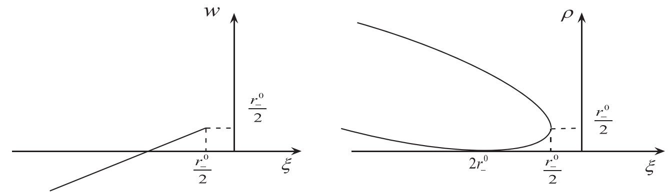

FIG. 2. The plots of the variables w, ρ in terms of the self-similar variable. The signs "±" of (75) indicate the different branches curve on the (ξ, ρ) plane.

For case (a), the variables ρ and w can be represented by r_-^0 as

$$\begin{aligned} w(\xi) &= \tfrac{1}{3}(\xi + r_-^0), \\ \rho(\xi) &= -\tfrac{1}{3}(\xi + r_-^0) \pm \sqrt{\tfrac{1}{3}r_-^0(2\xi - r_-^0)}. \end{aligned} \tag{75}$$

In order to make sure that the square root makes sense, it is necessary to set the condition $\xi \leqslant \frac{r_-^0}{2}$. The plots of the variables w and ρ with respect to the self-similar variable ξ, respectively, are shown in Fig. 2.

Similarly, for case (b), the variables ρ and w can be represented by r_+^0 as

$$\begin{aligned} w(\xi) &= \tfrac{1}{3}(\xi + r_+^0), \\ \rho(\xi) &= -\tfrac{1}{3}(\xi + r_+^0) \pm \sqrt{\tfrac{1}{3}r_+^0(2\xi - r_+^0)}. \end{aligned} \tag{76}$$

In practice, in order to make sure that the rarefaction wave solution is monotonic, the Riemann invariants should be single valued with respect to ξ. In this case, the rarefaction waves structure will satisfy the following boundary value conditions:

$$(a) \quad r_+^L < r_+^R, \quad r_-^L = r_-^R, \quad (b) \quad r_-^L < r_-^R, \quad r_+^L = r_+^R, \tag{77}$$

which are displayed in Fig. 3, in which the edge velocities can be formulated as follows:

$$\begin{aligned} &(a) \quad s_- = \tfrac{1}{2}r_-^L + \tfrac{3}{2}r_+^L, \qquad s_+ = \tfrac{1}{2}r_-^R + \tfrac{3}{2}r_+^R, \\ &(b) \quad s_- = \tfrac{3}{2}r_+^L + \tfrac{1}{2}r_-^L, \qquad s_+ = \tfrac{3}{2}r_+^R + \tfrac{1}{2}r_-^R. \end{aligned} \tag{78}$$

It is observed from Fig. 3 that the nonconstant Riemann invariant increases with the self-similar variable $\xi = x/t$.

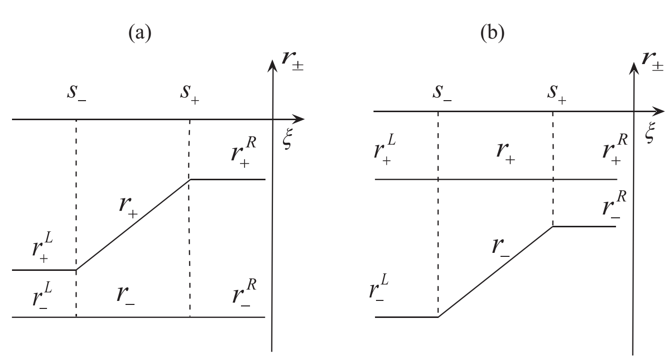

FIG. 3. The structures of the Riemann invariants $r_\pm$ with respect to $\xi = x/t$ under the boundary conditions in (77).

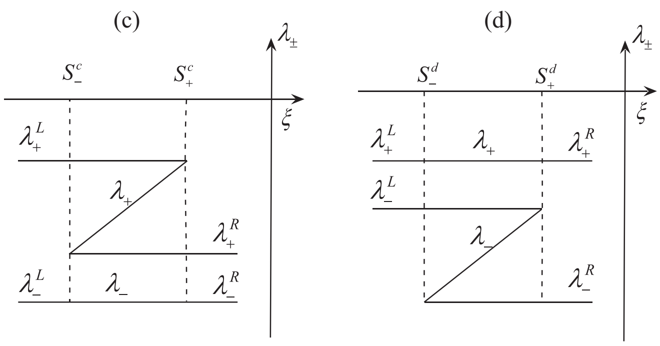

FIG. 4. The distributions of the Riemann invariants λ_i $(i = 1, 2, 3, 4)$ for the cnoidal dispersive shock wave.

However, the cases

$$\text{(c)}\quad r^L_+ > r^R_+,\quad r^L_- = r^R_-,\quad \text{(d)}\quad r^L_- > r^R_-,\quad r^L_+ = r^R_+, \tag{79}$$

do not correspond to rarefaction waves, but correspond to the cnoidal dispersive shock waves, which are investigated in the next section.

B. Cnoidal dispersive shock waves

This section studies the structures of the cnoidal dispersive shock waves [38,39]-[45,46], where the Riemann invariant is labeled by λ instead of r. So the two cases in (79) become

$$\text{(c)}\,\lambda^L_+ > \lambda^R_+,\quad \lambda^L_- = \lambda^R_-,\quad \text{(d)}\quad \lambda^L_- > \lambda^R_-,\ \lambda^L_+ = \lambda^R_+. \tag{80}$$

Note that the Riemann invariants λ_i $(i = 1, 2, 3, 4)$ satisfy the Whitham equation in (54), which can be used to describe the evolution of one-phase periodic waves and the dispersive shock wave. Hence, one can solve nonphysical multivalued problems, where the two nondispersion Riemann invariants $r_\pm$ can be replaced by the Riemann invariants λ_i $(i = 1, 2, 3, 4)$. When considering the self-similar variable $\xi = x/t$, the Whitham equation in (54) can be transformed into

$$(\nu_i - \xi)\frac{d\lambda_i}{dt} = 0,\quad i = 1, 2, 3, 4. \tag{81}$$

Through the discussion above, it is found that the three Riemann invariants are constants, and the remaining one (e.g., λ_j) changes in such a way that $\nu_j = \xi$. It is seen that the limiting form of the Whitham velocities in (56)–(58) is related closely to the dispersionless Riemann velocities in (70). Then one can find the relationship between λ_i and $r_\pm$, and the velocities at the edge of cnoidal dispersive shock waves. Figure 4 demonstrates the structures of the cnoidal dispersive shock waves. In Fig. 4(c), it is seen that

$$\lambda_1 = \lambda^L_+,\quad \lambda_3 = \lambda^R_+,\quad \lambda_4 = \lambda^L_- = \lambda^R_-, \tag{82}$$

while λ_2 changes according to the implicit equation

$$\nu_2(\lambda^L_+, \lambda_2, \lambda^R_+, \lambda^L_-) = \xi. \tag{83}$$

It is obvious that

$$\lambda^L_- = \tfrac{1}{2}r_-,\quad \lambda^L_+ = \tfrac{1}{2}r_+, \tag{84}$$

at the soliton edge of the cnoidal dispersive shock wave, while

$$\lambda^R_- = \tfrac{1}{2}r_-,\quad \lambda^R_+ = \tfrac{1}{2}r_+, \tag{85}$$

at the small-amplitude edge of the cnoidal dispersive shock wave. Moreover, velocities of the edges can be expressed by the Riemann invariants as follows:

$$\begin{aligned} s^c_- &= \lambda^L_+ + 2\lambda^R_+ + \lambda^L_-,\\ s^c_+ &= 4\lambda^L_+ + \frac{(\lambda^R_- - \lambda^R_+)^2}{2\lambda^L_+ - \lambda^R_+ - \lambda^R_-}. \end{aligned} \tag{86}$$

Similarly, in Fig. 4(d), one finds

$$\lambda_1 = \lambda^L_+ = \lambda^R_+,\quad \lambda_2 = \lambda^L_-,\quad \lambda_4 = \lambda^R_-, \tag{87}$$

while λ_3 changes according to the implicit equation

$$\nu_3(\lambda^R_+, \lambda^L_-, \lambda_3, \lambda^R_-) = \xi. \tag{88}$$

It is obvious that

$$\lambda^R_- = \tfrac{1}{2}r_-,\quad \lambda^R_+ = \tfrac{1}{2}r_+, \tag{89}$$

at the soliton edge of the cnoidal dispersive shock wave, while

$$\lambda^L_- = \tfrac{1}{2}r_-,\quad \lambda^L_+ = \tfrac{1}{2}r_+, \tag{90}$$

at the small-amplitude edge of the cnoidal dispersive shock wave. In a similar way, the Whitham velocities at the edges can be expressed by the Riemann invariants

$$\begin{aligned} s^d_- &= 4\lambda^R_- + \frac{(\lambda^R_+ - \lambda^L_-)^2}{\lambda^R_+ + \lambda^L_- - 2\lambda^R_-},\\ s^d_+ &= \lambda^R_+ + 2\lambda^L_- + \lambda^R_-. \end{aligned} \tag{91}$$

Substituting (82) or (87) into (50) and (51), respectively, it is found that the characteristic velocities v_i $(i = 1, 2, 3, 4)$ are dependent on ξ, which also means there exist two mappings from the Riemann invariants to the physical parameters. Therefore, each diagram of the Riemann invariant λ in Fig. 4 corresponds to two different cnoidal dispersive shock waves. For instance, for case (c), Fig. 5(a) shows that two parabolas, $\lambda^L_- = \lambda^R_- =$ const and $\lambda^L_+ =$ const, intersect at the points L_1 and L_2, which corresponds to the left boundary in Fig. 4(c). Two parabolas, $\lambda^L_- = \lambda^R_- =$ const and $\lambda^R_+ =$ const, intersect at the points R_1 and R_2, which corresponds to the right boundary in Fig. 4(c). Thus two paths from the left boundary to the right boundary are obtained, where $L_1 \to R_1$ and $L_2 \to R_2$ correspond to the two mappings (51) and (50), respectively. The analytical approximate solutions for the cnoidal dispersive

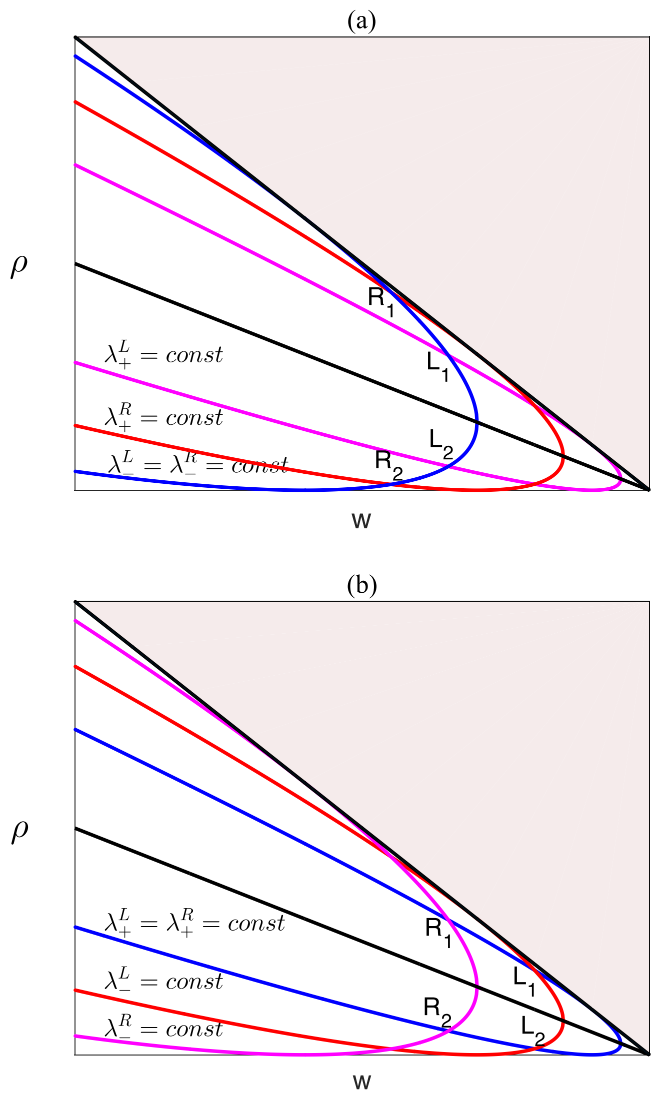

FIG. 5. The curves formed by the relationship between the variables ρ and w, where there exist two paths from the left boundary to the right boundary. (a) corresponds to case (c) and (b) corresponds to case (d).

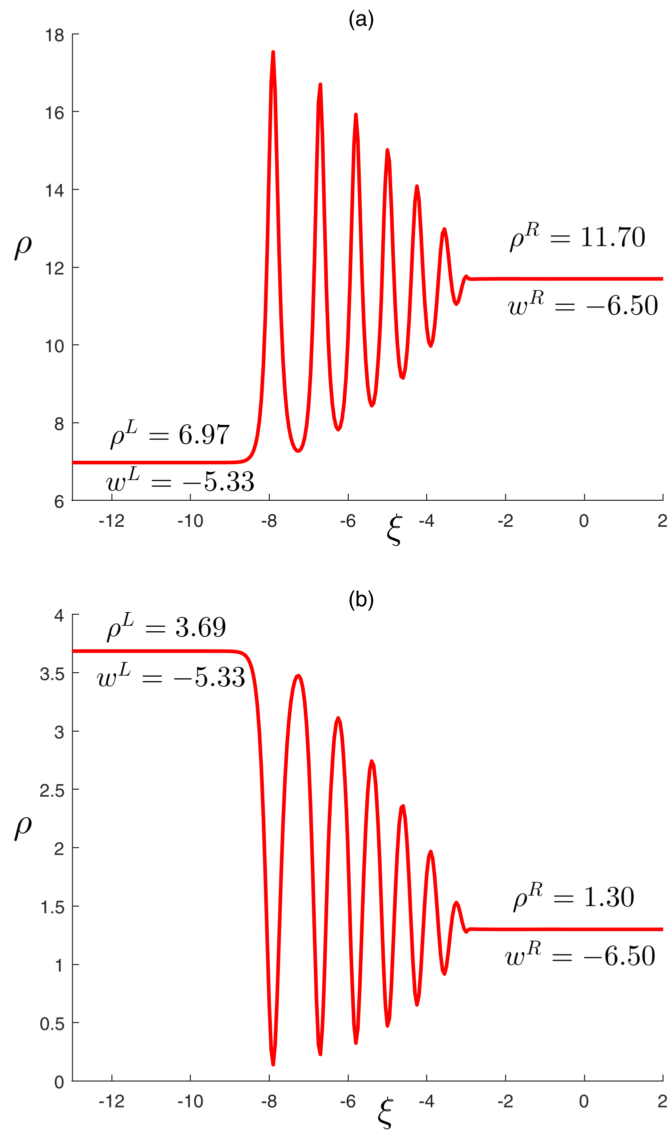

FIG. 6. The analytical approximation solution of the Gerdjikov-Ivanov equation (2) for two different boundary conditions corresponding to case (c) at $t = 2$, where the Riemann invariants are chosen as $\lambda_+^L = -0.13, \lambda_+^R = -1.3, \lambda_-^L = \lambda_-^R = -5.2$. (a) represents the boundary conditions $\rho^L = 6.97, w_L = -5.33, \rho^R = 11.70, w_R = -6.50$, while (b) represents the boundary conditions $\rho^L = 3.69, w_L = -5.33, \rho^R = 1.30, w_R = -6.50$.

shock waves are shown in Fig. 6, where Fig. 6(a) demonstrates the path from L_1 to R_1 in Fig. 5(a), and Fig. 6(b) demonstrates the path from L_2 to R_2 in Fig. 5(a). Similarly, for case (d), Fig. 5(b) shows that there also exist four intersection points of curves, which produces two paths, $L_1 \to R_1$ and $L_2 \to R_2$, in Fig. 5(b). The analytical approximate solutions for the cnoidal dispersive shock waves can also be obtained, which are displayed in Fig. 7.

C. Contact dispersive shock waves

In what follows, another basic wave structure is considered, in which the Riemann invariants have the same values at the boundaries, that is, $\lambda_+^L = \lambda_+^R$ and $\lambda_-^L = \lambda_-^R$. Thus the left and right boundary points (i.e., P_1 and P_2 in Fig. 8) locate in different monotonicity regions. Naturally, this produces a contact dispersive shock wave [38,39].

Figure 8 shows there are two paths that connect the two intersections P_1 and P_2 of the two parabolas. Note that the left and right boundary points appear on the opposite sides of the line $\rho = -w$. The Riemann invariants are displayed in Fig. 9, where the Riemann invariants λ_1 and λ_2 are equal, while the other two Riemann invariants λ_3 and λ_4 are constants, i.e., $\lambda_3 = \lambda_+^R = \lambda_+^L$, $\lambda_4 = \lambda_-^R = \lambda_-^L$. To be specific, one has $\lambda_1 = \lambda_2 = \lambda_+^L$ at the left edge and $\lambda_1 = \lambda_2 = 0$ at the right edge. Since $\lambda_1 = \lambda_2$, the modulus $m = 0$, so formula (58) indicates that the Whitham velocities can be expressed by

$$\nu_1 = \nu_2 = 4\lambda_1 - \frac{(\lambda_-^L - \lambda_+^L)^2}{2\lambda_1 - \lambda_+^L - \lambda_-^L} = \xi. \qquad (92)$$

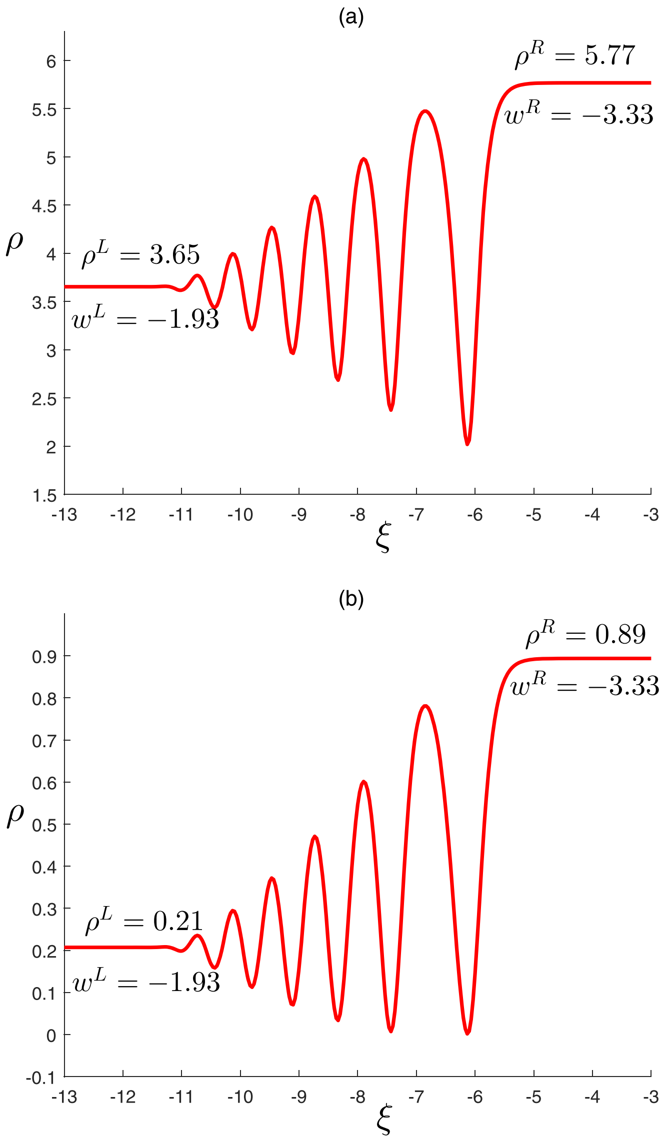

FIG. 7. The analytical approximation solution of the Gerdjikov-Ivanov equation (2) for two different boundary conditions corresponding to case (d) at $t = 2$, where the Riemann invariants are chosen as $\lambda_-^L = -1.4$, $\lambda_-^R = -2.8$, $\lambda_+^L = \lambda_+^R = -0.53$. (a) represents the boundary conditions $\rho^L = 3.65$, $w_L = -1.93$, $\rho^R = 5.77$, $w_R = -3.33$, while (b) represents the the boundary conditions $\rho^L = 0.21$, $w_L = -1.93$, $\rho^R = 0.89$, $w_R = -3.33$.

Moreover, the velocities of the edges are

$$s^L = v_3(\lambda_+^L, \lambda_+^L, \lambda_+^L, \lambda_-^L) = 3\lambda_+^L + \lambda_-^L,$$

$$s^R = v_2(0, 0, \lambda_+^R, \lambda_-^R) = \frac{(\lambda_-^L - \lambda_+^L)^2}{\lambda_+^L + \lambda_-^L}. \tag{93}$$

Following the same procedure for investigating the cnoidal dispersive shock waves, the different mappings (50) or (51) are chosen to demonstrate the basic wave structures corresponding to Fig. 9. Figure 10 displays two contact dispersive shock waves, where the wave structure in Fig. 10(a) is obtained by considering the path from P_1 to P_2 and the mapping (50), while Fig. 10(b) is obtained by using the path from P_2 to P_1 and the mapping (51).

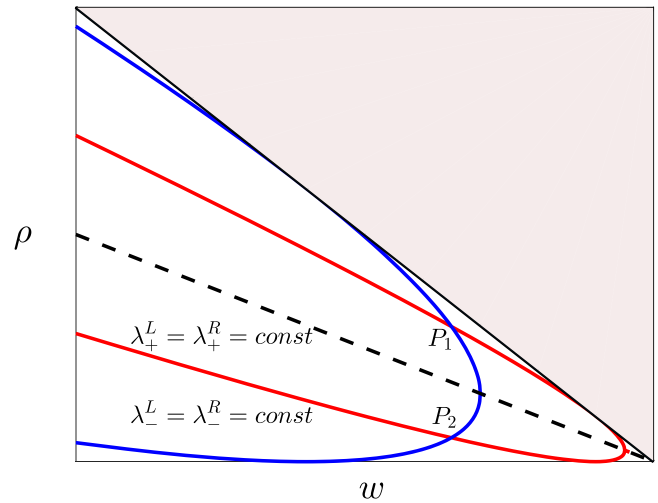

FIG. 8. The curves formed by the relationship between the variables ρ and w, in which the Riemann invariants have the same values at the boundaries. Here the paths $P_1 \to P_2$ and $P_2 \to P_1$ correspond to the two mappings (50) and (51), respectively.

D. Combined undular bores

This section considers the last basic wave structure, in which one Riemann invariant is constant, i.e., $\lambda_-^L = \lambda_-^R$, while the boundary values of the other Riemann invariants are not equal as in [38,39]. In this case, the left and right boundary points locate in different regions of the (w, ρ) plane, which are displayed in Fig. 11. Obviously, there arise two edge cases of the form

$$\text{(a)} \quad \lambda_+^L > \lambda_+^R, \quad \text{(b)}\, \lambda_+^L < \lambda_+^R. \tag{94}$$

In this case, the transition $P_1 \to P_2$ in Fig. 8 can be generalized into two different ways represented in Fig. 11. Figure 11(a) shows the path $L_1 \to R_1$ and Fig. 11(b) shows the path $L_2 \to R_2$. The distributions of the Riemann invariants corresponding to the two paths in Fig. 11 are demonstrated in Fig. 12, which results in novel combined undular bores in Fig. 13. It is observed from Figs. 12(a) and 13(a) that

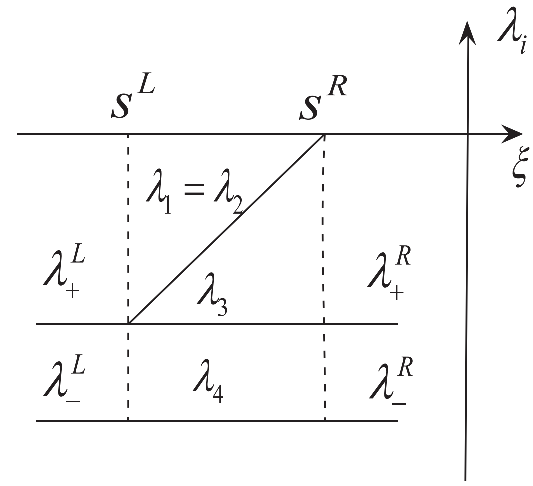

FIG. 9. The distribution of the Riemann invariants λ_i ($i = 1, 2, 3, 4$) for the contact dispersive shock wave.

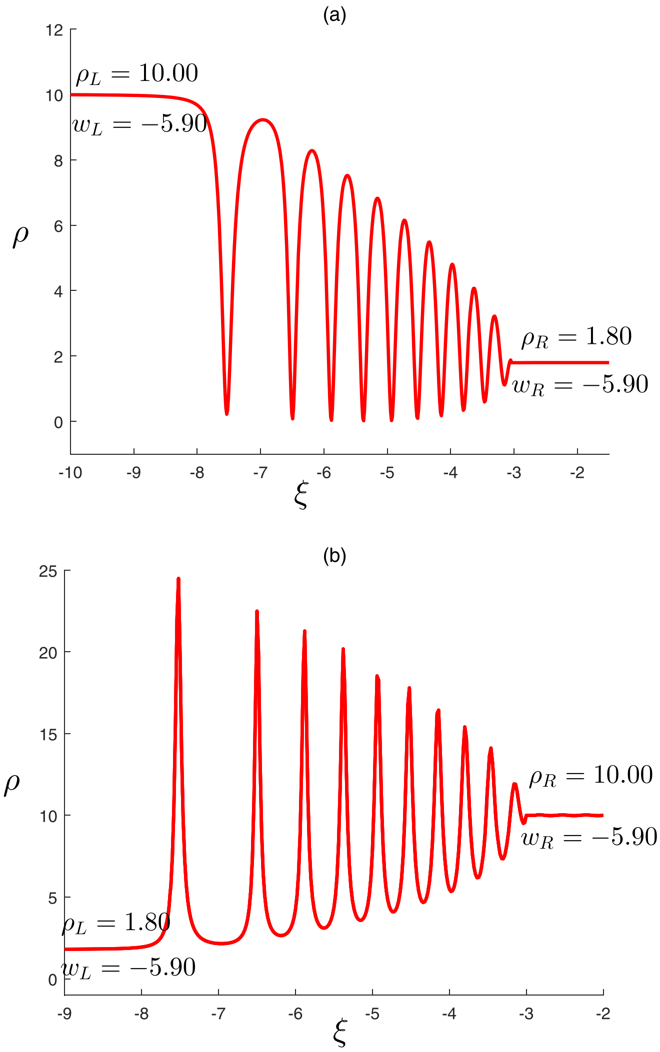

FIG. 10. The analytical approximation solution of the Gerdjikov-Ivanov equation (2) for two paths, $P_1 \to P_2$ and $P_2 \to P_1$, in Fig. 8 for $t = 5$, where the boundary condition for (a) is $\rho^L = 10.00$, $w_L = -5.90$, $\rho^R = 1.80$, $w_R = -5.90$ and the boundary condition for (b) is $\rho^L = 1.80$, $w_L = -5.90$, $\rho^R = 5.80$, $w_R = -5.90$. Here the Riemann invariants are chosen as $\lambda_+^L = \lambda_+^R = -0.83$, $\lambda_-^L = \lambda_-^R = -5.07$.

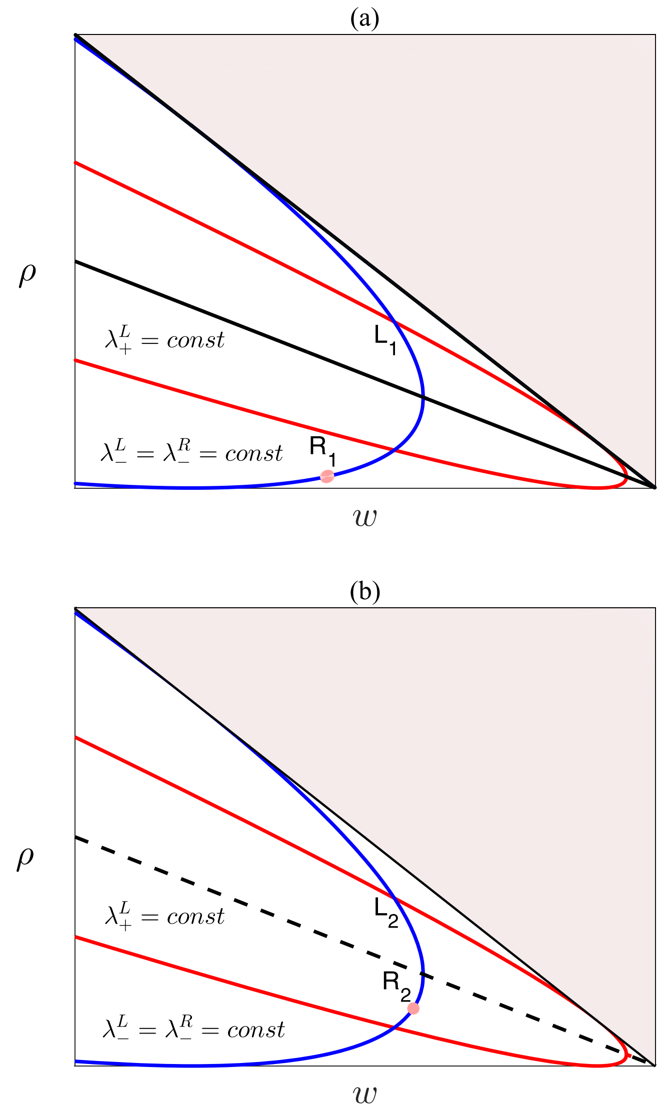

FIG. 11. The curves formed by the relationship between the variables ρ and w, where there exist two paths from the left boundary to the right boundary. (a) corresponds to case (a) in (94) and (b) corresponds to case (b) in (94).

the combined undular bore consists of a cnoidal dispersive shock wave and a contact dispersive shock wave. However, Figs. 12(b) and 13(b) show that the combined undular bore consists of a rarefaction wave and a contact dispersive shock wave [38,39].

In the limit $m \to 1$, there occurs a dark soliton at the soliton front S_1^a, while in the limit $m \to 0$, a trigonometric wave and a small-amplitude edge occur at the harmonic fronts S_2^a and S_3^a, respectively (see Figs. 12 and 13 for details). The Whitham velocities at the boundaries of Fig. 12(a) can be expressed by

$$
\begin{aligned}
s_1^a &= v_2(\lambda_+^L, \lambda_+^R, \lambda_+^R, \lambda_-^L) = \lambda_+^L + 2\lambda_+^R + \lambda_-^L,\\
s_2^a &= v_2(\lambda_+^L, \lambda_+^L, \lambda_+^R, \lambda_-^R) = 4\lambda_+^L + \frac{(\lambda_-^R - \lambda_+^R)^2}{2\lambda_+^L - \lambda_+^R - \lambda_-^R},\\
s_3^a &= v_1(0, 0, \lambda_+^R, \lambda_-^R) = -\frac{(\lambda_-^R - \lambda_+^R)^2}{\lambda_+^R + \lambda_-^R}.
\end{aligned}
\tag{95}
$$

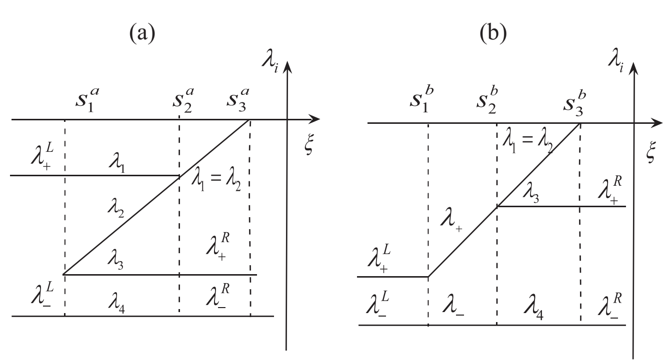

FIG. 12. The distributions of the Riemann invariants λ_i ($i = 1, 2, 3, 4$) for the combined undular bores corresponding to the two paths in Fig. 11.

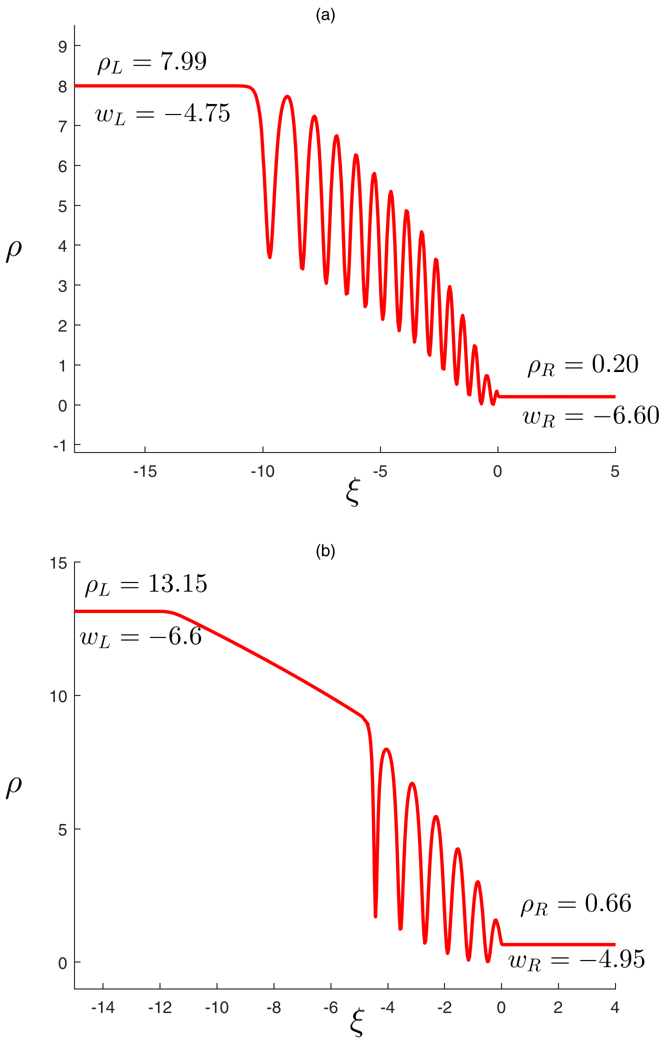

FIG. 13. The analytical approximation solution of the Gerdjikov-Ivanov equation (2) for two paths, $L_1 \to R_1$ and $L_2 \to R_2$, in Fig. 11 for $t = 2$, where the boundary condition for (a) is $\rho^L = 7.99$, $w_L = -4.75$, $\rho^R = 0.20$, $w_R = -6.60$ and the Riemann invariants are chosen as $\lambda_+^L = -0.64$, $\lambda_+^R = -2.49$, $\lambda_-^L = \lambda_-^R = -4.11$. The boundary condition for (b) is $\rho^L = 13.15$, $w_L = -6.60$, $\rho^R = 0.66$, $w_R = -4.95$, and the Riemann invariants are chosen as $\lambda_+^L = -2.89$, $\lambda_+^R = -1.24$, $\lambda_-^L = \lambda_-^R = -3.71$.

In a similar way, the Whitham velocities at the boundaries of Fig. 12(b) can be expressed by

$$s_1^b = 3\lambda_+^L + \lambda_-^L,$$
$$s_2^b = 3\lambda_+^R + \lambda_-^R,$$
$$s_3^b = \nu_2(0, 0, \lambda_+^R, \lambda_-^R) = -\frac{(\lambda_-^R - \lambda_+^R)^2}{\lambda_+^R + \lambda_-^R}. \quad (96)$$

Up to now, four basic wave structures of the Gerdjikov-Ivanov equation (2) with the discontinuous initial value condition (59)-(60) are discussed in detail. In what follows, the complete classification of the optical undular bores in this problem are proposed.

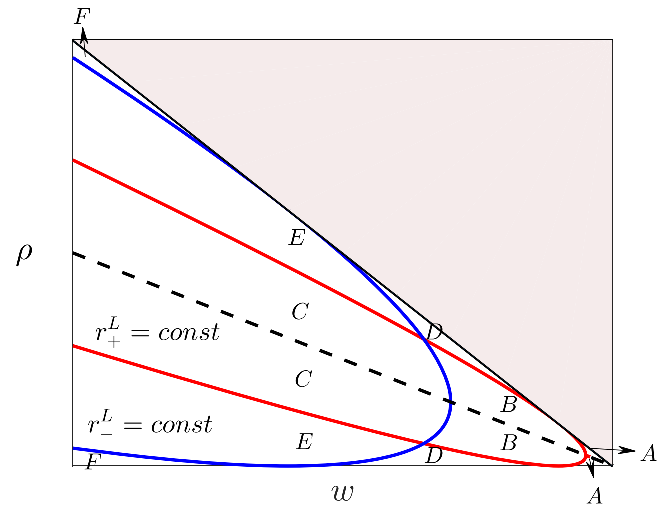

FIG. 14. Six regions in the (w, ρ) plane corresponding to different structures of optical undular bores, where the intersection of the parabolas $\rho = -w \pm \sqrt{r_+^L(2w - r_+^L)}$ and $\rho = -w \pm \sqrt{r_-^L(2w - r_-^L)}$ corresponds to the left boundary.

IV. CLASSIFICATION OF THE OPTICAL UNDULAR BORES

In order to give the complete classification of the optical undular bores in the Riemann problem of the Gerdjikov-Ivanov equation (2), the relationship between the variables w and ρ in (72) are used to partition the (w, ρ) plane (see Fig. 14), where the line $\rho = -w$ divides the (w, ρ) plane into two monotonicity regions. It is seen that there are six regions in the (w, ρ) plane, which are marked as $A, B, \ldots, F$ and satisfy the following order relations [38,39]:

$$A: \quad \lambda_-^L < \lambda_+^L < \lambda_-^R < \lambda_+^R; \quad B: \quad \lambda_-^L < \lambda_-^R < \lambda_+^L < \lambda_+^R;$$

$$C: \quad \lambda_-^R < \lambda_-^L < \lambda_+^L < \lambda_+^R; \quad D: \quad \lambda_-^L < \lambda_-^R < \lambda_+^R < \lambda_+^L;$$

$$E: \quad \lambda_-^R < \lambda_-^L < \lambda_+^R < \lambda_+^L; \quad F: \quad \lambda_-^R < \lambda_+^R < \lambda_-^L < \lambda_+^L.$$

Case A. The order relation $\lambda_-^L < \lambda_+^L < \lambda_-^R < \lambda_+^R$.

In such case, no dispersive shock wave appears. Figure 15 shows that there exist five regions, in which the left and right platforms (regions I and V) are connected by two rarefaction waves (regions II and IV), and the middle region (region III) is a vacuum region. Figure 15(a) displays the the Riemann invariants and Figs. 15(b) and 15(c) show the the wave patterns of the fluid density ρ and fluid velocity w, respectively. Notice that the relationship between ρ and w is given in the Appendix. The Whitham velocities of the edges for each region are listed below:

$$S_A = v_-(\lambda_+^L, \lambda_-^L) = \lambda_+^L + 3\lambda_-^L,$$
$$S_B = v_+(\lambda_+^L, \lambda_+^L) = 4\lambda_+^L,$$
$$S_C = v_-(\lambda_-^R, \lambda_-^R) = 4\lambda_-^R,$$
$$S_D = v_+(\lambda_+^R, \lambda_-^R) = 3\lambda_+^R + \lambda_-^R. \quad (97)$$

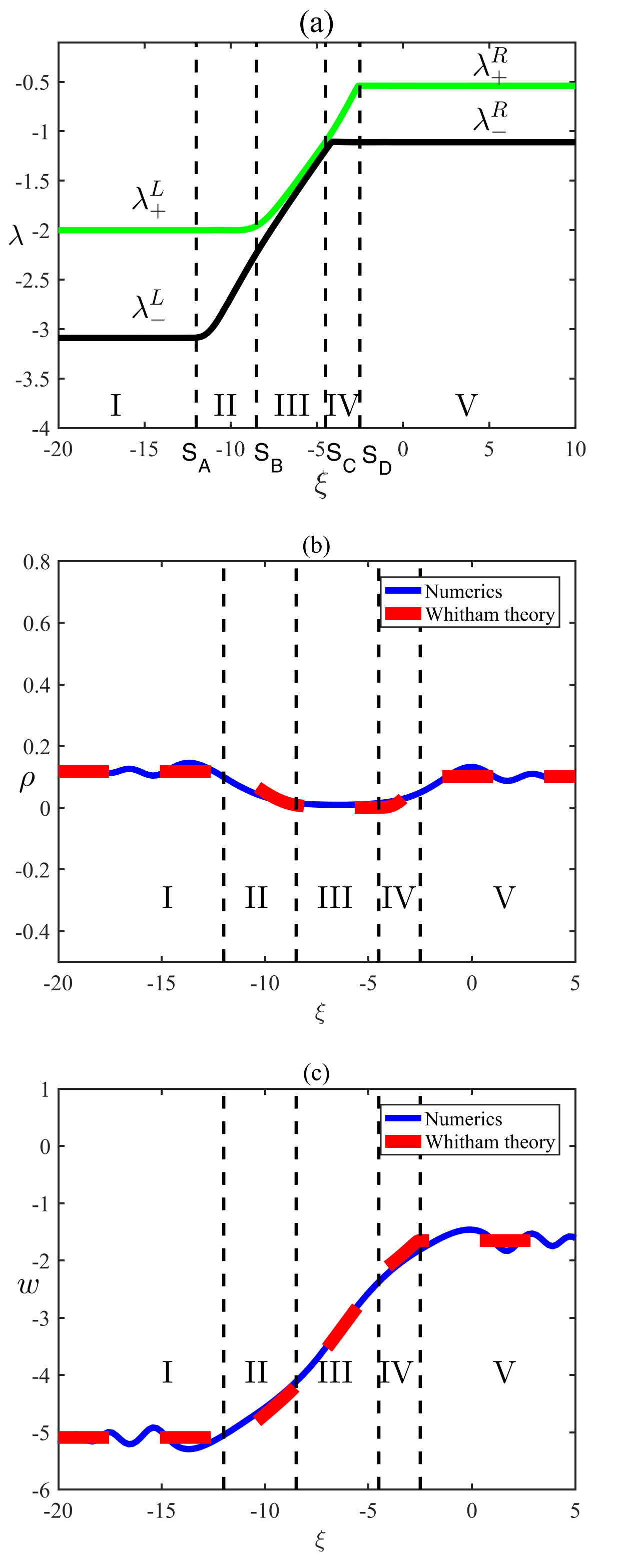

FIG. 15. The structures of the Riemann invariants and solution of the Gerdjikov-Ivanov equation (2) in case A at $t = 1$. (a) represents the evolution of the Riemann invariants in terms of the variable ξ, and (b) and (c) display the wave patterns of the density function ρ and velocity function w from Whitham theory (thick red) and numerical calculations (thin blue), respectively. Here, the parameters are $\lambda_+^L = -2, \lambda_-^L = -3.09, \lambda_+^R = -0.54, \lambda_-^R = -1.11$.

Case B. The order relation $\lambda_-^L < \lambda_-^R < \lambda_+^L < \lambda_+^R$. As in case *A*, no dispersive shock wave appears in this case. In addition, different from case *A*, no vacuum region exists in case *B*. It is observed from Fig. 16 that there are also five regions, which are platform, rarefaction wave, platform, rarefaction wave, and platform from left to right. The boundary velocities in each region are expressed by

$$\begin{aligned} S_A &= v_-(\lambda_+^L, \lambda_-^L) = \lambda_+^L + 3\lambda_-^L, \\ S_B &= v_-(\lambda_+^L, \lambda_-^R) = \lambda_+^L + 3\lambda_-^R, \\ S_C &= v_+(\lambda_+^L, \lambda_-^R) = 3\lambda_+^L + \lambda_-^R, \\ S_D &= v_+(\lambda_+^R, \lambda_-^R) = 3\lambda_+^R + \lambda_-^R. \end{aligned} \tag{98}$$

Case C. The order relation $\lambda_-^R < \lambda_-^L < \lambda_+^L < \lambda_+^R$.

In this case, there appears a dispersive shock wave with four Riemann invariants. It is seen from Fig. 17 that five regions emerge, which are platform, dispersive shock wave, platform, rarefaction wave, and platform from left to right. The boundary velocities in each region are given by

$$\begin{aligned} S_A &= v_3(\lambda_+^L, \lambda_-^L, \lambda_-^R, \lambda_-^R) = 4\lambda_-^R + \frac{(\lambda_+^L - \lambda_-^L)^2}{\lambda_+^L + \lambda_-^L - 2\lambda_-^R}, \\ S_B &= v_3(\lambda_+^L, \lambda_-^L, \lambda_-^L, \lambda_-^R) = \lambda_+^L + 2\lambda_-^L + \lambda_-^R, \\ S_C &= v_+(\lambda_+^L, \lambda_-^R) = 3\lambda_+^L + \lambda_-^R, \\ S_D &= v_+(\lambda_+^R, \lambda_-^R) = 3\lambda_+^R + \lambda_-^R. \end{aligned} \tag{99}$$

Case D. The order relation $\lambda_-^L < \lambda_-^R < \lambda_+^R < \lambda_+^L$.

The case *D* in Fig. 18 is similar to Case *C*. However, the locations of the regions are opposite to case *C*, which from left to right are platform, rarefaction wave, platform, dispersive shock wave, and platform, respectively. The Riemannian invariants of the rarefaction wave correspond to the distribution in Fig. 3(b), while the Riemannian invariants of the dispersive shock wave correspond to the distribution in Fig. 4(c). The boundary velocities in each region are given by

$$\begin{aligned} S_A &= v_-(\lambda_+^L, \lambda_-^L) = 3\lambda_-^L + \lambda_+^L, \\ S_B &= v_-(\lambda_+^L, \lambda_-^R) = 3\lambda_-^R + \lambda_+^L, \\ S_C &= v_2(\lambda_+^L, \lambda_+^R, \lambda_+^R, \lambda_-^R) = \lambda_+^L + 2\lambda_+^R + \lambda_-^R, \\ S_D &= v_2(\lambda_+^L, \lambda_+^L, \lambda_+^R, \lambda_-^R) = 4\lambda_+^L + \frac{(\lambda_-^R - \lambda_+^R)^2}{2\lambda_+^L - \lambda_+^R - \lambda_-^R}. \end{aligned} \tag{100}$$

Case E. The order relation $\lambda_-^R < \lambda_-^L < \lambda_+^R < \lambda_+^L$.

This is a case in which two dispersive shock waves are connected by a middle platform (see Fig. 19). No rarefaction wave exists in this case. The regions from left to right are

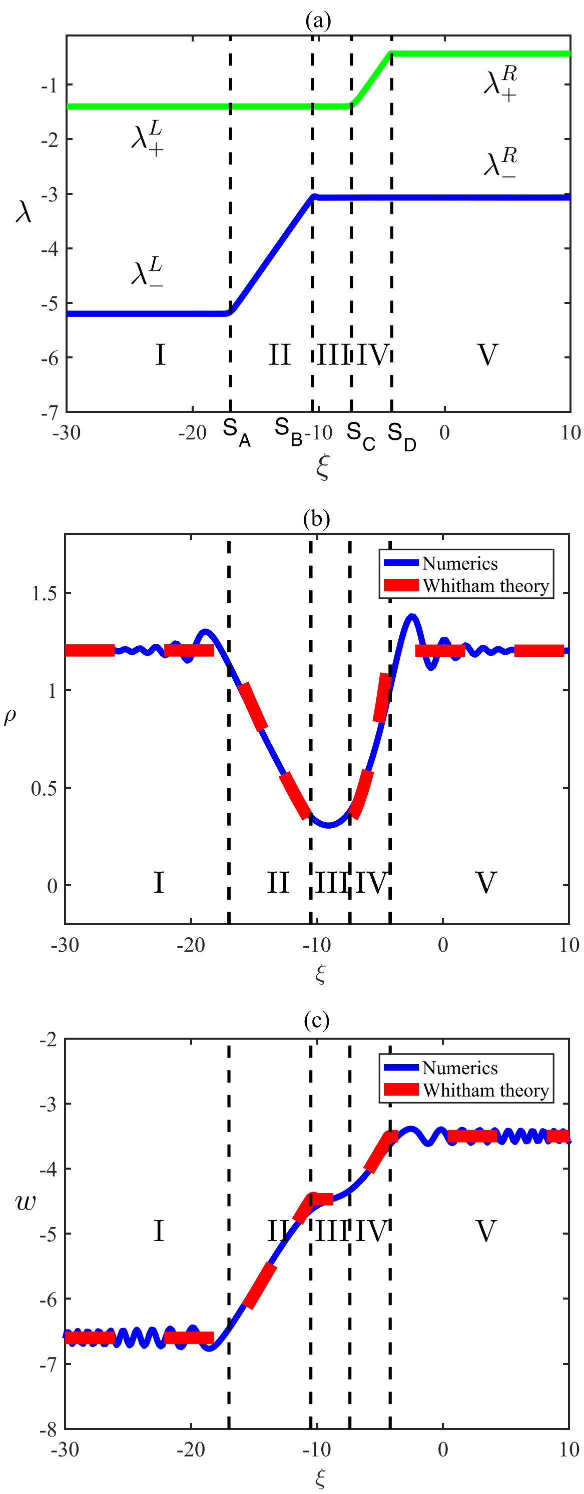

FIG. 16. The structures of the Riemann invariants and solution of the Gerdjikov-Ivanov equation (2) in case B at $t = 1$. (a) represents the evolution of the Riemann invariants in terms of the variable ξ, and (b) and (c) display the wave patterns of the density function ρ and velocity function w from Whitham theory (thick red) and numerical calculations (thin blue), respectively. Here, the parameters are $\lambda_+^L = -1.40$, $\lambda_-^L = -5.20$, $\lambda_+^R = -0.43$, $\lambda_-^R = -3.07$.

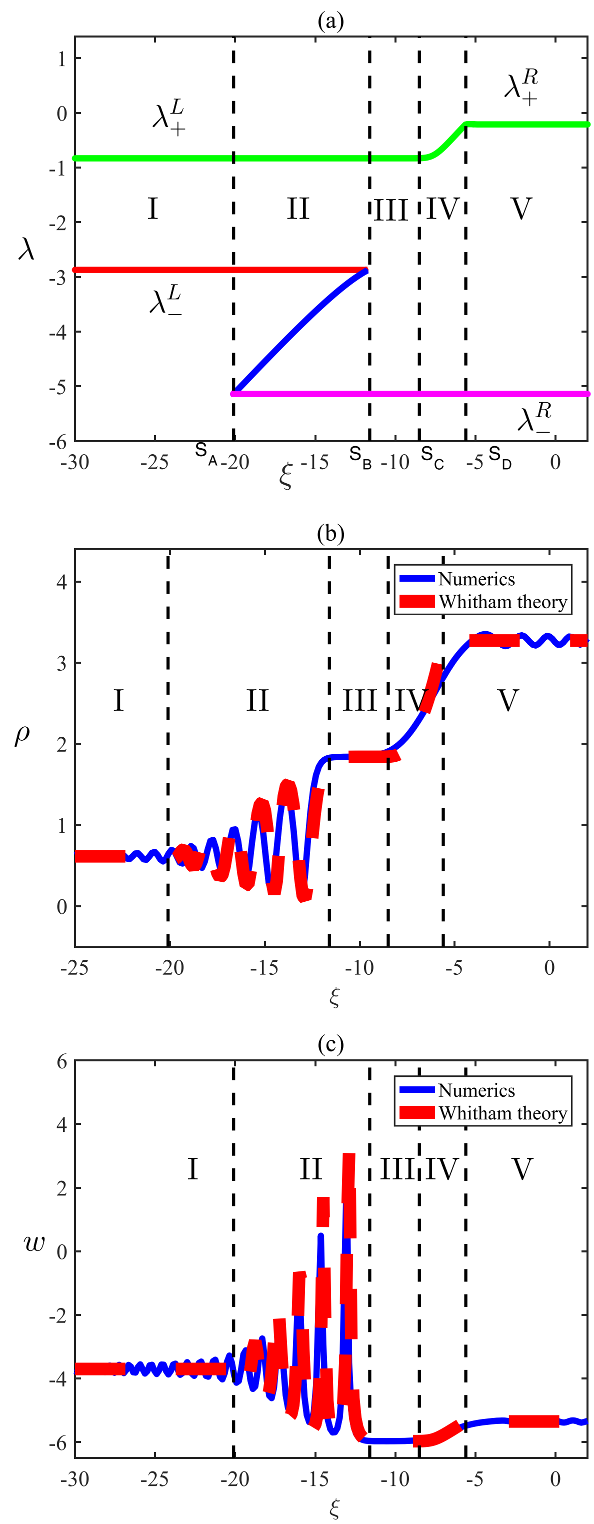

FIG. 17. The structures of the Riemann invariants and solution of the Gerdjikov-Ivanov equation (2) in case C at $t = 1$. (a) represents the evolution of the Riemann invariants in terms of the variable ξ, and (b) and (c) display the wave patterns of the density function ρ and velocity function w from Whitham theory (thick red) and numerical calculations (thin blue), respectively. Here, the parameters are $\lambda_+^L = -0.83$, $\lambda_-^L = -2.87$, $\lambda_+^R = -0.21$, $\lambda_-^R = -5.14$.

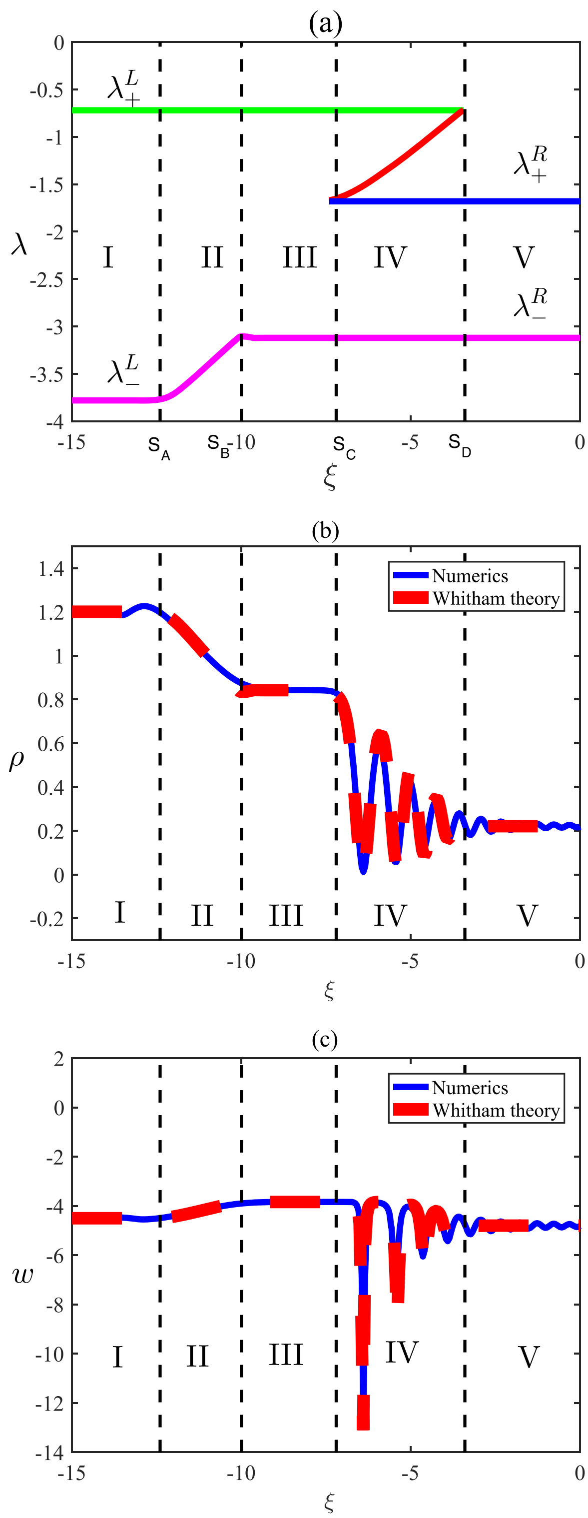

FIG. 18. The structures of the Riemann invariants and solution of the Gerdjikov-Ivanov equation (2) in case D at $t = 3$. (a) represents the evolution of the Riemann invariants in terms of the variable ξ, and (b) and (c) display the wave patterns of the density function ρ and velocity function w from Whitham theory (thick red) and numerical calculations (thin blue), respectively. Here, the parameters are $\lambda_+^L = -0.72$, $\lambda_-^L = -3.78$, $\lambda_+^R = -1.68$, $\lambda_-^R = -3.12$.

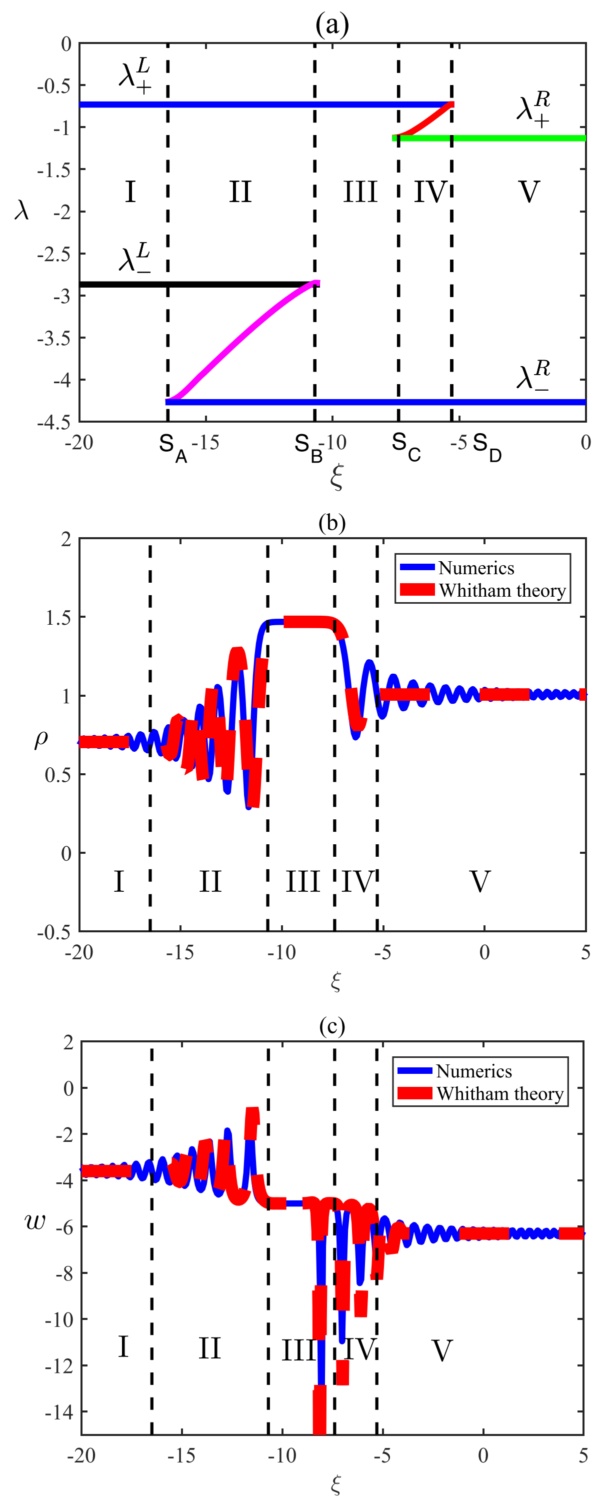

FIG. 19. The structures of the Riemann invariants and solution of the Gerdjikov-Ivanov equation (2) in case E at $t = 2$. (a) represents the evolution of the Riemann invariants in terms of the variable ξ, and (b) and (c) display the wave patterns of the density function ρ and velocity function w from Whitham theory (thick red) and numerical calculations (thin blue), respectively. Here, the parameters are $\lambda_+^L = -0.73$, $\lambda_-^L = -2.87$, $\lambda_+^R = -1.13$, $\lambda_-^R = -4.27$.

platform, dispersive shock wave, platform, dispersive shock wave, and platform, respectively. The boundary velocities in each region are given by

$$S_A = v_3(\lambda_+^L, \lambda_-^L, \lambda_-^R, \lambda_-^R) = 4\lambda_-^R + \frac{(\lambda_+^L - \lambda_-^L)^2}{\lambda_+^L + \lambda_-^L - 2\lambda_-^R},$$
$$S_B = v_3(\lambda_+^L, \lambda_-^L, \lambda_-^L, \lambda_-^R) = \lambda_+^L + 2\lambda_-^L + \lambda_-^R,$$
$$S_C = v_2(\lambda_+^L, \lambda_+^R, \lambda_+^R, \lambda_-^R) = \lambda_+^L + 2\lambda_+^R + \lambda_-^R,$$
$$S_D = v_2(\lambda_+^L, \lambda_+^L, \lambda_+^R, \lambda_-^R) = 4\lambda_+^L + \frac{(\lambda_-^R - \lambda_+^R)^2}{2\lambda_+^L - \lambda_+^R - \lambda_-^R}. \quad (101)$$

Case F. The order relation $\lambda_-^R < \lambda_+^R < \lambda_-^L < \lambda_+^L$.

This is a case containing three dispersive shock waves, in which one dispersive shock wave is a nonmodulated cnoidal dispersive shock wave. The five regions are represented in Fig. 20, which from left to right are platform, dispersive shock wave, nonmodulated dispersive shock wave, dispersive shock wave, and platform, respectively. It is seen from Fig. 20(a) that the four Riemann invariants for the nonmodulated dispersive shock wave (region III) are constants, which are called hard edges. This is the unique property of the defocusing system such as the defocusing NLS equation. The boundary velocities in each region are given by

$$S_A = v_3(\lambda_+^L, \lambda_-^L, \lambda_-^R, \lambda_-^R) = 4\lambda_-^R + \frac{(\lambda_+^L - \lambda_-^L)^2}{\lambda_+^L + \lambda_-^L - 2\lambda_-^R},$$
$$S_B = v_3(\lambda_+^L, \lambda_-^L, \lambda_+^R, \lambda_-^R),$$
$$S_C = v_2(\lambda_+^L, \lambda_-^L, \lambda_+^R, \lambda_-^R),$$
$$S_D = v_2(\lambda_+^L, \lambda_+^L, \lambda_+^R, \lambda_-^R) = 4\lambda_+^L + \frac{(\lambda_-^R - \lambda_+^R)^2}{2\lambda_+^L - \lambda_+^R - \lambda_-^R}. \quad (102)$$

Finally, it is remarked that when the boundary points lie in the monotone region with $\rho > -w$ in Fig. 14, similar to the previous analysis, one can also get six regions with the same order of Riemann invariants. Based on the location of the right boundary points in a certain region, the corresponding wave structures can also be proposed, which coincide with those for the previous case.

V. CONCLUSIONS

In conclusion, the Riemann problem of the Gerdjikov-Ivanov equation governing the photon fluid with quintic nonlinearity has been studied by means of the Whitham theory. The algebro-geometric solution and the Whitham equations corresponding to the one-phase periodic solution are formulated. Then the main basic wave structures of the Riemann problem are found such as the rarefaction waves, the cnoidal dispersive shock waves, the contact dispersive shock waves, and the combined undular bores. Finally, the solution classification of the Riemann problem of the Gerdjikov-Ivanov equation is discussed and many exotic optical undular bores are found. It is worthwhile noting that all the results from Whitham theory are verified by full numerical simulations.

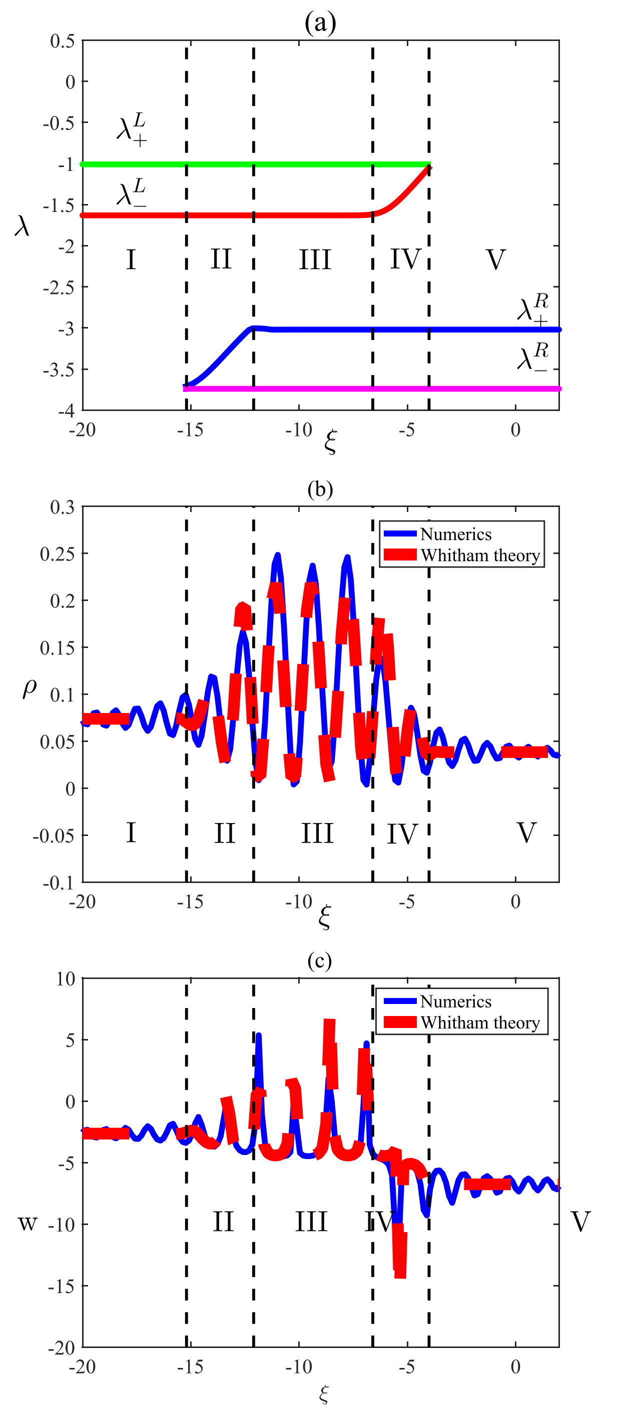

FIG. 20. The structures of the Riemann invariants and solution of the Gerdjikov-Ivanov equation (2) in case F at $t = 1$. (a) represents the evolution of the Riemann invariants in terms of the variable ξ, and (b) and (c) display the wave patterns of the density function ρ and velocity function w from Whitham theory (thick red) and numerical calculations (thin blue), respectively. Here, the parameters are $\lambda_+^L = -1.01$, $\lambda_-^L = -1.63$, $\lambda_+^R = -3.02$, $\lambda_-^R = -3.54$.

ACKNOWLEDGMENT

This work was supported by National Natural Science Foundation of China through Grants No. 11971067 and No. 12371247, and the Fundamental Research Funds for the Central Universities through Grant No. 2020NTST22.

APPENDIX

This Appendix considers the traveling-wave solution of the hydrodynamic system (62) by taking the traveling-wave transformation

$$\rho(x,t)=\rho(\xi),\quad w(x,t)=w(\xi),\quad \xi=x-Vt.$$

In this case, the following ordinary differential equations are derived:

$$-V\rho_\xi+2\rho_\xi w+2\rho w_\xi+\rho\rho_\xi=0, \tag{A1}$$

$$-Vw_\xi+2ww_\xi-(\rho w)_\xi-\rho\rho_\xi = \frac{1}{\sqrt{\rho}}\left(\frac{\rho_{\xi\xi}}{2\sqrt{\rho}}-\frac{\rho_\xi^2}{4\rho^{\frac{3}{2}}}\right)_\xi. \tag{A2}$$

Integrating Eq. (A1) once, yields

$$w=\frac{1}{2}V-\frac{1}{4}\rho+\frac{C}{2\rho}, \tag{A3}$$

where C is an integral constant. Substituting (A3) into (A2) gives

$$-\frac{3}{8}\rho\rho_\xi-\frac{c^2\rho_\xi}{2\rho^3}-\frac{1}{2}V\rho_\xi=\left(\frac{\rho_{\xi\xi}}{2\rho}-\frac{\rho_\xi^2}{4\rho^2}\right)_\xi. \tag{A4}$$

Then integrating Eq. (A4), one has

$$-\frac{3}{16}\rho^2+\frac{c^2}{4\rho^2}-\frac{1}{2}V\rho=\left(\frac{\rho_{\xi\xi}}{2\rho}-\frac{\rho_\xi^2}{4\rho^2}\right)_\xi+B, \tag{A5}$$

where B is an integral constant. Multiplying the above equation by ρ_ξ, integrating it and introducing the integral constant A, we have

$$\rho_\xi^2=-\tfrac{1}{4}\rho^4-V\rho^3-4B\rho^2-4A\rho-C^2 \tag{A6}$$

$$=-\tfrac{1}{4}(\rho-\rho_1)(\rho-\rho_2)(\rho-\rho_3)(\rho-\rho_4), \tag{A7}$$

where $\rho_1,\rho_2,\rho_3,\rho_4$ are real roots of the algebraic equation $\frac{1}{4}\rho^4+V\rho^3+4B\rho^2+4A\rho-C^2=0$ satisfying $\rho_1\leqslant\rho_2\leqslant\rho_3\leqslant\rho_4$. In this case, Eq. (A6) coincides with the previous equation (25). Thus the four constants $A,\ B,\ C,$ and U can be expressed by ρ_i $(i=1,2,3,4)$ as

$$A=-\frac{1}{16}\sum_{i<j<s}\rho_i\rho_j\rho_s,\quad B=\frac{1}{16}\sum_{i<j}\rho_i\rho_j, \tag{A8}$$

$$C=\pm\frac{1}{2}\sqrt{\rho_1\rho_2\rho_3\rho_4},\quad V=-\frac{1}{4}\sum_{i=1}^{4}\rho_i. \tag{A9}$$

It is obvious that

$$\rho_1\leqslant\rho\leqslant\rho_2,\quad \rho_3\leqslant\rho\leqslant\rho_4, \tag{A10}$$

which permits one to get the real solutions for Eq. (A6). To be specific, for $\rho_1\leqslant\rho\leqslant\rho_2$, the traveling-wave solution is obtained as

$$\rho(\xi)=\frac{\rho_2(\rho_4-\rho_1)-\rho_4(\rho_2-\rho_1)\mathrm{cn}^2(\omega,m)}{\rho_4-\rho_2+(\rho_2-\rho_1)\mathrm{sn}^2(\omega,m)}, \tag{A11}$$

$$w(\xi)=\frac{1}{2}V-\frac{1}{4}\rho+\frac{C}{2\rho}, \tag{A12}$$

where $\omega=\sqrt{(\rho_3-\rho_1)(\rho_4-\rho_2)}\xi/4$ and

$$m=\frac{(\rho_4-\rho_3)(\rho_2-\rho_1)}{(\rho_4-\rho_2)(\rho_3-\rho_1)}. \tag{A13}$$

When $\rho_3\leqslant\rho\leqslant\rho_4$, another traveling-wave solution is obtained as

$$\rho=\frac{\rho_3(\rho_1-\rho_4)+\rho_1(\rho_4-\rho_3)\mathrm{cn}^2(\omega,m)}{\rho_1-\rho_3+(\rho_3-\rho_4)\mathrm{sn}^2(\omega,m)}, \tag{A14}$$

$$w=\frac{1}{2}V-\frac{1}{4}\rho+\frac{C}{2\rho}, \tag{A15}$$

where $\omega=\sqrt{(\rho_3-\rho_1)(\rho_4-\rho_2)}\xi/4$ and

$$m=\frac{(\rho_4-\rho_3)(\rho_2-\rho_1)}{(\rho_4-\rho_2)(\rho_3-\rho_1)}. \tag{A16}$$

[1] G. A. El, R. H. J. Grimshaw, and N. F. Smyth, Unsteady undular bores in fully nonlinear shallow-water theory, Phys. Fluids **18**, 027104 (2006).

[2] R. H. Clarke, R. K. Smith, and D. G. Reid, The morning glory of the Gulf of Carpentaria: An atmospheric undular bore, Mon. Weather Rev. **109**, 1726 (1981).

[3] P. A. Madsen, D. R. Fuhrman, and H. A. Schäffer, On the solitary wave paradigm for tsunamis, J. Geophys. Res.: Oceans **113**, 12012 (2008).

[4] M. A. Hoefer, M. J. Ablowitz, I. Coddington, E. A. Cornell, P. Engels, and V. Schweikhard, Dispersive and classical shock waves in Bose-Einstein condensates and gas dynamics, Phys. Rev. A **74**, 023623 (2006).

[5] R. Z. Sagdeev, The fine structure of a shock wave front propagated across a magnetic field in a rarefied plasma, Sov. Phys. Tech. Phys. **6**, 867 (1962).

[6] G. Xu, M. Conforti, A. Kudlinski, A. Mussot, and S. Trillo, Dispersive Dam-Break Flow of a Photon Fluid, Phys. Rev. Lett. **118**, 254101 (2017).

[7] A. M. Kamchatnov, *Nonlinear Periodic Waves and Their Modulations—An Introductory Course* (World Scientific, Singapore, 2000).

[8] G. A. El and M. A. Hoefer, Dispersive shock waves and modulation theory, Phys. D (Amsterdam, Neth.) **333**, 11 (2016).

[9] S. K. Ivanov and A. M. Kamchatnov, Formation of dispersive shock waves in evolution of a two-temperature collisionless plasma, Phys. Fluids **32**, 126115 (2020).

[10] J. Fatome, C. Finot, G. Millot, A. Armaroli, and S. Trillo, Observation of Optical Undular Bores in Multiple Four-Wave Mixing, Phys. Rev. X **4**, 021022 (2014).

[11] G. B. Whitham, Nonlinear dispersive waves, Proc. R. Soc. London, Ser. A **283**, 238 (1965).

[12] G. B. Whitham, *Linear and Nonlinear Waves* (Wiley, New York, 1974).

[13] A. V. Gurevich and L. P. Pitaevskii, Nonstationary structure of a collisionless shock wave, Zh. Eksp. Teor. Fiz. **65**, 590 (1973) [Sov. Phys. - JETP **38**, 291 (1974)].

[14] J. C. Luke, A perturbation method for nonlinear dispersive wave problems, Proc. R. Soc. London, Ser. A **292**, 403 (1966).

[15] M. J. Ablowitz and D. J. Benney, The evolution of multi-phase modes for nonlinear dispersive waves, Stud. Appl. Math. **49**, 225 (1970).

[16] H. Flaschka, M. G. Forest, and D. W. McLaughlin, Multiphase averaging and the inverse spectral solution of the Korteweg–de Vries equation, Commun. Pure Appl. Math. **33**, 739 (1980).

[17] B. A. Dubrovin and S. P. Novikov, Hydrodynamics of weakly deformed soliton lattices. Differential geometry and Hamiltonian theory, Russ. Math. Surv. **44**, 35 (1989).

[18] *Spatial Solitons*, edited by S. Trillo and W. Torruellas (Springer, Berlin, Heildelberg, 2001), Vol. 82.

[19] N. Karjanto and E. van Groesen, Note on wavefront dislocation in surface water waves, Phys. Lett. A **371**, 173 (2007).

[20] B. D. Josephson, The discovery of tunnelling supercurrents, Rev. Mod. Phys. **46**, 251 (1974).

[21] F. Dalfovo, S. Giorgini, L. P. Pitaevskii, and S. Stringari, Theory of Bose-Einstein condensation in trapped gases, Rev. Mod. Phys. **71**, 463 (1999).

[22] A. V. Gurevich and A. L. Krylov, Dissipationless shock waves in media with positive dispersion, Soy. Phys. JETP **65**, 944 (1987).

[23] A. V. Gurevich, A. L. Krylov, and G. A. El, Quasilongitudinal nonlinear dispersing MHD waves, Sov. Phys. JETP **75**, 825 (1992).

[24] G. A. El, V. V. Geogjaev, A. V. Gurevich, and A. L. Krylov, Decay of an initial discontinuity in the defocusing NLS hydrodynamics, Phys. D (Amsterdam, Neth.) **87**, 186 (1995).

[25] D. J. Kaup and A. C. Newell, An exact solution for a derivative nonlinear Schrödinger equation, J. Math. Phys. **19**, 798 (1978).

[26] H. H. Chen, Y. C. Lee, and C. S. Liu, Integrability of nonlinear Hamiltonian systems by inverse scattering method, Phys. Scr. **20**, 490 (1979).

[27] V. S. Gerdjikov and M. I. Ivanov, The quadratic bundle of general form and the nonlinear evolution equations, Bulg. J. Phys. **10**, 130 (1983).

[28] A. Kundu, Landau-Lifshitz and higher-order nonlinear systems gauge generated from nonlinear Schrödinger-type equations, J. Math. Phys. **25**, 3433 (1984).

[29] B. L. Lawrence, M. Cha, J. U. Kang, W. Toruellas, G. Stegeman, G. Baker, J. Meth, and S. Etemad, Large purely refractive nonlinear index of single crystal P-toluene sulphonate (PTS) at 1600 nm, Electron. Lett. **30**, 447 (1994).

[30] G. Boudebs, S. Cherukulappurath, H. Leblond, J. Troles, F. Smektala, and F. Sanchez, Experimental and theoretical study of higher-order nonlinearities in chalcogenide glasses, Opt. Commun. **219**, 427 (2003).

[31] P. A. Clarkson and C. M. Cosgrove, Painlevé analysis of the nonlinear Schrödinger family of equations, J. Phys. A: Math. Gen. **20**, 2003 (1987).

[32] E. Fan, Integrable evolution systems based on Gerdjikov-Ivanov equations, bi-Hamiltonian structure, finite-dimensional integrable systems and N-fold Darboux transformation, J. Math. Phys. **41**, 7769 (2000).

[33] A. Biswas, Y. Yildirim, E. Yasar, and M. M. Babatin, Conservation laws for Gerdjikov-Ivanov equation in nonlinear fiber optics and PCF, Optik **148**, 209 (2017).

[34] X. Lü, W. X. Ma, J. Yu, F. Lin, and C. M. Khalique, Envelope bright- and dark-soliton solutions for the Gerdjikov-Ivanov model, Nonlinear Dyn. **82**, 1211 (2015).

[35] E. Fan, Darboux transformation and soliton-like solutions for the Gerdjikov-Ivanov equation, J. Phys. A: Math. Gen. **33**, 6925 (2000).

[36] J. Xu, E. Fan, and Y. Chen, Long-time asymptotic for the derivative nonlinear Schrödinger equation with step-like initial value, Math. Phys. Anal. Geom. **16**, 253 (2013).

[37] N. A. Kudryashov, Traveling wave solutions of the generalized Gerdjikov-Ivanov equation, Optik **219**, 165193 (2020).

[38] S. K. Ivanov and A. M. Kamchatnov, Riemann problem for the photon fluid: Self-steepening effects, Phys. Rev. A **96**, 053844 (2017).

[39] S. K. Ivanov, Riemann problem for the light pulses in optical fibers for the generalized Chen-Lee-Liu equation, Phys. Rev. A **101**, 053827 (2020).

[40] F. Gesztesy and H. Holden, *Soliton Equations and Their Algebro-Geometric Solutions*, *Vol. I:* $(1+1)$*-Dimensional Continuous Models*, Cambridge Studies in Advanced Mathematics Vol. 79 (Cambridge University Press, Cambridge, 2003).

[41] E. R. Tracy and H. H. Chen, Nonlinear self-modulation: An exactly solvable model, Phys. Rev. A **37**, 815 (1988).

[42] V. P. Kotlyarov and A. R. Its, Periodic problem for the nonlinear Schrödinger equation, Dopov. Akad. Nauk Ukr RSR, Ser. A **11**, 965 (1976) (in Ukrainian), arXiv:1401.4445.

[43] E. D. Belokolos, A. I. Bobenko, V. Z. Enol'skii, A. R. Its, and V. B. Matveev, *Algebro-Geometric Approach to Nonlinear Integrable Equations* (Springer-Verlag, Berlin, Heidelberg, 1994).

[44] M. Abramowitz and I. A. Stegun, *Handbook of Mathematical Functions* (Dover Publ., New York, 1972).

[45] D. S. Wang, L. Xu, and Z. Xuan, The complete classification of solutions to the Riemann problem of the defocusing complex modified KdV equation, J. Nonlinear Sci. **32**, 3 (2022).

[46] R. Z. Gong and D. S. Wang, Whitham modulation theory of defocusing nonlinear Schrödinger equation and the classification and evolutions of solutions with initial discontinuity, Acta Phys. Sin. **72**, 100503 (2023).

[47] J. C. DiFranco and P. D. Miller, The semiclassical modified nonlinear Schrödinger equation I: Modulation theory and spectral analysis, Phys. D (Amsterdam, Neth.) **237**, 947 (2008).